Article:
Cosgrove, GIE, Poyatos-Moré, M, Lee, DR et al. (2020) Intra-clinothem variability in sedimentary texture and process regime recorded down slope profiles. Sedimentology, 67 (1). pp. 431-456. ISSN: 0037-0746

https://doi.org/10.1111/sed.12648

Intra-clinothem variability in sedimentary texture and process regime recorded down slope profiles

LIST OF AUTHORS: GRACE I.E. COSGROVE[1]*, MIQUEL POYATOS-MORÉ[2], DAVID LEE[1], DAVID M. HODGSON[1], WILLIAM D. McCAFFREY[1], NIGEL P. MOUNTNEY[1]

LIST OF ADDRESSES:

[1]School of Earth and Environment, University of Leeds, Leeds LS2 9JT, United Kingdom

[2]Department of Geosciences, University of Oslo, 0371 Oslo, Norway

***CORRESPONDING AUTHOR:** eegiec@leeds.ac.uk

Associate Editor – Massimiliano Ghinassi

Short Title – Intra-clinothem variability down slope profiles

ABSTRACT

Shelf-margin clinothem successions can archive process interactions at the shelf to slope transition, and their architecture provides constraints on the interplay of factors that control basin-margin evolution. However, detailed textural analysis and facies distributions from shelf to slope transitions remain poorly documented. This study uses quantitative grain-size and sorting data from coeval shelf and slope deposits of a single clinothem that crops out along a 5 km long, dip-parallel transect of the Eocene Sobrarbe Deltaic Complex (Ainsa Basin, south-central Pyrenees, Spain). Systematic sampling of sandstone beds tied to measured sections has captured vertical and basinward changes in sedimentary texture and facies distributions at an intra-clinothem scale. Two types of hyperpycnal flow, related slope deposits, both rich in mica and terrestrial organic matter, are differentiated according to grain size, sorting and bed geometry: (i) sustained hyperpycnal flow deposits, which are physically linked to coarse channelised sediments in the shelf setting and which deposit sand down the complete slope profile; (ii)

episodic hyperpycnal flow deposits, which are disconnected from, and incise into, shelf sands and which are associated with sediment bypass of the proximal slope and coarse-grained sand deposition on the medial and distal slope. Both types of hyperpycnites are interbedded with relatively homogenous, organic-free and mica-free, well-sorted, very fine-grained sandstones, which are interpreted to be remobilised from wave-dominated shelf environments; these wave-dominated deposits are found only on the proximal and medial slope. Coarse-grained sediment bypass into the deeper-water slope settings is therefore dominated by episodic hyperpycnal flows, whilst sustained hyperpycnal flows and turbidity currents remobilizing wave-dominated shelf deposits are responsible for the full range of grain-sizes in the proximal and medial slope, thus facilitating clinoform progradation. This novel dataset highlights previously undocumented intra-clinothem variability related to updip changes in the shelf process-regime, which is therefore a key factor controlling downdip architecture and resulting sedimentary texture.

INTRODUCTION

Clinothems typically form progradational basin margin successions (e.g. Gilbert, 1885; Rich, 1951; Asquith, 1970; Mitchum et al., 1977; Pirmez et al., 1998; Adams & Schlager, 2000; Bhattacharya, 2006; Patruno et al., 2015). Seismic reflection and well-log data have been used extensively to study subsurface clinothem successions (e.g. Ross et al., 1995; Pinous et al., 2001; Donovan, 2003; Jennette et al., 2003; Hadler-Jacobsen et al., 2005). However, outcrop examples of clinothems offer a higher-resolution record of stratigraphic and downslope clinothem evolution (e.g. Helland-Hansen, 1992; Dreyer et al., 1999; Pyles & Slatt, 2007; Pontén & Plink-Björklund, 2009; Hubbard et al., 2010; Dixon et al., 2012a; Jones et al., 2013; Poyatos-Moré et al., 2019). Exhumed clinothem successions provide the opportunity to document patterns of facies distribution and sedimentary texture. This information can be used to help constrain the interplay of controls on clinothem evolution (e.g. Mellere et al., 2002; Plink-Björklund & Steel, 2003; Carvajal & Steel, 2006; Pyles & Slatt, 2007; Jones et al., 2015; Laugier & Plink-Björklund, 2016). However, predicting facies distributions and sedimentary textures within individual clinothems, both vertically and along depositional dip, remains challenging (Cosgrove et al., 2018). In part, this is due to the lack of detailed, quantitative grain size and sorting datasets recovered from clinothem sequences, which has left down-clinothem changes in grain size and sorting as poorly constrained and largely unquantified parameters (Catuneanu et al., 2009).

Prediction of sedimentary texture along a continuous clinothem depositional profile is further complicated by changes in the dominant shelf process-regime (cf. Dixon et al., 2012b; Laugier & Plink-Björklund, 2016; Cosgrove et al., 2018). Process-regime affects how and when sediment of different calibre and maturity is transferred downdip (Dixon et al., 2012b; Cosgrove et al., 2018). Sudden changes in shelf process-regime can occur over intra-clinothem timescales (Ta et al., 2002; Ainsworth et al., 2008; Plink-Björklund, 2008; Carvajal & Steel, 2009; Vakarelov & Ainsworth, 2013; Jones et al., 2015). Despite this, mixed-energy clinothems systems are under-represented in the literature (see Ainsworth et al., 2011; Olariu, 2014; Rossi & Steel, 2016) and clinothems are therefore commonly designated as being end-member types (i.e. river-dominated, wave-dominated or tide-dominated, systems) (e.g. Dreyer et al., 1999; Pink-Björklund et al., 2001; Plink-Björklund & Steel, 2002; Deibert et al., 2003; Crabaugh & Steel, 2004; Plink-Björklund & Steel, 2004; Johannessen & Steel, 2005; Petter & Steel, 2006; Sylvester et al., 2012). As such, the impact of mixed process-regime conditions on downslope sedimentary texture remains relatively understudied (e.g. Cosgrove et al., 2019).

To improve understanding of process and textural variability within individual clinothem sequences, this study focuses on the Sobrarbe Deltaic Complex, an outcrop example of well-constrained clinothems, located in the Eocene Ainsa Basin, south-central Pyrenees, Spain (Fig. 1). This system is ideal for studying quantitative changes in grain size and sorting at high spatial resolution, due to the presence of a series of well-exposed and accessible clinothem sequences, which can be directly correlated from coeval fluvio-deltaic shelf to distal slope deposits (Dreyer et al., 1999). This investigation uses detailed facies analyses and quantitative changes in grain size and sorting to address three overarching questions: (i) how do changes in the dominant shelf process regime affect facies distribution within an individual clinothem sequence; (ii) how do changes in sedimentary texture (including grain size and sorting) vary up-stratigraphy and along depositional dip; and (iii) can quantitative grain-size data be used to identify sediment bypass at the clinoform rollover? This outcrop-based study provides new insights into the evolution of individual clinothems and may be used as a predictive reference for subsurface exploration and basin evolution models.

GEOLOGICAL SETTING

The Sobrarbe Deltaic Complex crops out in the western part of the Eocene Ainsa Basin, north-eastern Spain (Fig. 1). The Ainsa Basin in the Upper Eocene is a piggyback basin, located in and on top of the easternmost portion of the Gavarnie thrust-sheet-complex, and forms the central sector of the South

Pyrenean foreland basin (Vergés & Muñoz, 1990; Muñoz, 1992; Fernández et al., 2004). The Ainsa Basin is bordered to the west by the Jaca-Pamplona Basin and to the east by the Tremp-Graus Basin (Puigdefàbregas, 1975; Brunet, 1986). The western part of the basin is characterised by several fold structures that were active during deposition: the Añisclo anticline to the north; the Peña Montañesa thrust to the north-east; the Mediano anticline to the east; the Boltaña anticline to the west (Fig. 2; Poblet et al., 1998; Dreyer et al., 1999; Fernández et al., 2004; 2012).

The fill of the western Ainsa Basin is dominated by a *ca* 5 km thick succession of Upper Eocene sediments. As part of these, the Sobrarbe Deltaic Complex (typically *ca* 800 m thick) comprises the uppermost part of the San Vicente Formation (marly slope deposits and turbiditic sandstones), the Sobrarbe Formation (shallow-marine deposits), and up to the middle part of Mondot Member of the Escanilla Formation (alluvial red-bed succession) (Van Lunsen, 1970; DeFrederico, 1981; Dreyer et al., 1993; Wadsworth, 1994). These deltaic successions accumulated over a period of *ca* 3 Myr during the middle Lutetian to lower Bartonian, reaching a maximum thickness of *ca* 1 km (Muñoz et al., 1998).

The Sobrarbe Deltaic Complex comprises a series of well-exposed, *ca* 100 m thick clinothems, which crop-out in a >5 km long transect, in an approximately dip-parallel orientation. These clinothems show the transition from fluvio-deltaic deposits (Escanilla Formation) in the south to progressively deeper shelf- and slope-deposits (Sobrarbe and San Vicente formations) in the north (Dreyer et al., 1999). Dreyer et al. (1999) subdivided the Sobrarbe Deltaic Complex into five composite sequences: the Comaron, the Las Gorgas, the Barranco el Solano, the Buil and the Mondot Member of the Escanilla Formation (Fig. 3). These composite sequences are separated by major unconformities, which represent fluctuations in relative sea-level (Dreyer et al., 1999).

The composite sequences are in turn subdivided into 'minor sequences' (Dreyer et al., 1999), which comprise sandstones units interbedded with mudstones and marls. The minor sequences are described as genetic sequences, bounded by transgressive surfaces (*sensu* Galloway, 1989). The first minor sequence of the Las Gorgas composite sequence is the specific focus of this study (Fig. 3).

METHODS AND TERMINOLOGY

The term clinoform is used to describe sinusoidal basinward-dipping chronostratigraphic stratal surfaces, whereas the term clinothem is used to describe the sedimentary packages that occur between these surfaces (e.g. Gilbert, 1885; Rich, 1951; Mitchum et al., 1977; Pirmez et al., 1998; Patruno et al.,

2015). Clinothems are typically composed of three constituent parts: a geometric shelf (topset deposits; updip, gently basinward dipping), a geometric slope (foreset deposits; central component, seaward-dipping typically at *ca* 1 to 3°) and a geometric basin-floor (bottomset deposits; downdip, gently dipping) (Gilbert, 1885; Steel & Olsen, 2002). The zone of the clinoform rollover denotes an area of gradient increase and is the site of the uppermost break-in-slope between the shelf and slope segments (Van Wagoner et al., 1990; Pirmez et al., 1998; Plink-Björklund et al., 2001; Glørstad-Clark et al., 2010, Glørstad-Clark et al., 2011; Anell & Midtkandal, 2015; Jones et al., 2015). Clinothems develop at scales ranging from subaerial delta clinothems (*ca* tens of metres in height), to basin-margin clinothems (ranging from *ca* hundreds of metres to >1 km in height) (e.g. Pirmez et al., 1998; Steel & Olsen, 2002; Helland-Hansen & Hampson 2009; Henriksen et al., 2009; Anell & Midtkandal, 2015; Patruno et al., 2015; Patruno & Helland Hansen, 2018).

The rock samples used in this investigation were acquired from the oldest clinothem of the Las Gorgas composite sequence (Figs 2 and 3), hereafter referred to as Cycle LG-1 (Fig. 4), which is continuously exposed in depositional dip for *ca* 5 km and which reveals a shelf to slope transect. In Cycle LG-1, seven sample locations were chosen along the continuous depositional profile to provide even down-dip coverage of the shelf to slope transition (Fig. 4).

At each sampling site, detailed sedimentary logs were collected, and between four and seven rock samples were recovered. In total, 36 samples were recovered from Cycle LG-1. The locations of the rock samples were recorded using a handheld GPS and photographed; georeferenced sample locations are included in the Supplementary Material. To ensure consistency and repeatability, and to avoid impact of mudstone clasts, rock samples were recovered from *ca* 0.1 m above the base of each sandstone-package.

Small blocks (*ca* 25 mm x 25 mm x 10 mm) were cut from each rock sample; samples were then polished and impregnated with epoxy resin, carbon-coated and placed on a scanning electron microscope (SEM) mount using conductive copper tape. Photomicrographs of samples were taken using a Tescan SEM (Tescan, Brno–Kohoutovice, Czech Republic) at the University of Leeds Electron Microscopy and Spectroscopy Centre. All SEM photomicrographs were taken in backscatter mode at a similar contrast to ensure comparability. The photomicrographs were imported into the image processing and analysis program ImageJ, which was used to identify grain boundaries and to calculate grain diameters (e.g. Sumner et al., 2012). Measured grain-diameters ascertained from thin section, or photomicrographs, are

smaller than the true maximum grain diameter (e.g. Chayes, 1950, Greenman, 1951; Kellerhals et al., 1975). However, due to the fully-lithified nature of the recovered rock-samples, photomicrograph analysis was deemed to be the most effective grain-sizing methodology. The statistical analysis of all ImageJ results was completed using GRADISTAT computer software (Blott & Pye 2001), which enables the rapid analysis of grain-size and sorting statistics (e.g. St-Onge et al., 2004; Gammon et al., 2017).

Extensive unmanned aerial vehicle (UAV) photography was collected. Using georeferenced photographs, acquired using a DJI Phantom 3, a photorealistic three-dimensional outcrop model was constructed using the photogrammetric software Agisoft PhotoScan. The resulting model was analysed using the LIME visualisation software (www.virtualoutcrop.com). UVA-footage has enabled the construction of a high-resolution outcrop model, in which Cycle LG-1 can be traced laterally and the sampling locations can be illustrated (Fig. 4).

CLINOTHEM GEOMETRY

The large-scale and well-exposed nature of the Sobrarbe Deltaic Complex allows the palaeo-bathymetric position of the shelf, clinoform rollover and slope to be constrained (Fig. 4). Clinothem gradients, as outlined below, are averaged from UAV digital outcrop models (Fig. 4), which represent compacted stratigraphy.

Description

From Location 1 to 2, Cycle LG-1 has sub-horizontal geometry. From Location 2 to 3, there is an increase in average clinoform gradient, from sub-horizontal to *ca* 4°, associated with an increase in clinothem thickness (Fig. 4). From Location 3 to 4 there is an increase in average clinothem gradient to *ca* 8°. From Location 4 to 6 there is a decrease in average clinothem gradient to *ca* 5 °. From Location 6 to 7, average clinothem gradient decreases to *ca* 2° (Fig. 4).

Interpretation

The relatively flat clinothem geometry observed from Location 1 to 2 suggests a shelf (topset) environment (e.g. Steel & Olsen, 2002; Patruno et al., 2015; Laugier & Plink-Björklund, 2016). The prominent increase in gradient from Location 2 to 3 is interpreted to define the zone of clinothem rollover (e.g. Pirmez et al., 1998; Glørstad-Clark et al., 2010; Anell & Midtkandal, 2015); this is further

supported by the prominent stratigraphic thickening (Fig 4B; cf. Dixon et al.., 2012b). Thus, Locations 4 to 7, associated with a basinward-dipping profile, represent slope deposits (e.g. Van Wagoner et al., 1990; Pirmez et al., 1998; Plink-Björklund et al., 2001; Glørstad-Clark et al., 2010). The slope is further sub-divided into proximal, medial and distal locations, based on proximity to the clinoform rollover and slope gradient. The most steeply-dipping portion of the clinothem (represented by Location 4), is therefore interpreted as the proximal slope; the medial slope is represented by Locations 5 and 6, and is associated with a minor gradient-decrease; the distal slope (represented by Location 7) is associated with a further gradient decrease (e.g. Steel & Olsen, 2002; Glørstad-Clark et al., 2010; Anell & Midtkandal, 2015). This clinoform geometry interpretation is supported by the distribution of facies, as outlined below.

FACIES ASSOCIATIONS AND DISTRIBUTION

Five facies associations have been determined within Cycle LG-1, which are distinguishable by differences in sedimentary structure, bed-scale architecture, bed geometry and quantitative differences in grain size and sorting.

Shelf Deposits

Facies Association A: fluvial channel-fill deposits

Description (see Table 1)

Facies Association A (FA A) is predominantly composed of fine-grained and medium-grained sandstone (34% and 31%, respectively, Fig. 5A) with a mean grain size of 0.34 mm (medium-grained sand; Fig. 6A). This FA has a large intra-facies grain-size variability, and can be locally very coarse-grained, although it is generally moderately well-sorted (1.50 σ mean sorting; Fig. 6B). Typically, grains are subangular to rounded. FA A varies from 0.25 to 18.0 m in thickness (Fig. 7), and has a highly discontinuous, lenticular geometry (Fig. 8A). The base of FA A is erosional, cutting up to 0.5 m deep into underlying siltstones (Fig. 8B). The base of FA A is often associated with mudstone rip-up clasts. Facies Association A typically shows a fining-upward trend and is bounded by flat to concave-up surfaces. Sedimentary structures include planar and trough cross-stratification; rare asymmetrical current ripple cross-lamination is observed. Typically, cross-strata sets are 0.5 to 1.0 m thick, and dip uniformly; sets are bounded by flat surfaces, which dip in the same direction as the cross-beds (Fig. 8C). Sandstones can contain sub-

rounded granules and pebbles (20 to 50 mm in size) of extraformational origin concentrated at the base of FA A, or parallel to stratification, which are dominantly quartz, with subordinate feldspar and lithic clasts (Fig. 8D). Locally, plant matter is present as detritus. Disarticulated and fragmented bivalve shells form a hash that is found as scour-fill. Facies Association A crops out in Locations 1 and 2, stratigraphically thickening towards Location 2 (Figs 4 and 7).

Interpretation

The presence of lenticular sand bodies, bounded by basal erosion surfaces and containing decimetre-scale cross-bedding with dominant unidirectional palaeocurrents indicates a channel-fill environment for FA A (Farrell, 1987; Collinson et al., 2006); the fluvial nature of the infill is further supported by the presence of terrestrial plant fragments and detritus. The bivalve hash is interpreted to be reworked from underlying deposits. The planar and trough cross-stratified sedimentary structures record the migration of dune-scale bedforms, and the occurrence of basal granules and pebbles indicates relative high-energy conditions. The fining-upward trends suggest progressive flow velocity decrease during the channel infill (e.g. Williams & Rust, 1969; Bridge et al., 1986). The channel-fill interpretation is further supported by the location of FA A within the geometric shelf-environment.

Facies Association B: delta top overbank deposits

Description (see Table 1)

Facies Association B (FA B) is predominantly composed of very fine and fine-grained sandstone (54% and 32%, respectively, Fig. 5B), and has a mean grain size of 0.10 mm (very fine-grained sand; Fig. 6A). This FA is moderately sorted (1.73 σ mean sorting; Fig. 6B), with subrounded grains. Bedsets are 1 to 2 m thick, and composed of 0.05 to 0.1 m thick and relatively tabular sandstone beds, interbedded with thin (0.05 to 0.2 m thickness) structureless siltstones (Fig. 8E). The sandstone and siltstone units are found interbedded with organic-rich mudstones (0.2 to 1.0 m thick). Tabular sandstone beds have sharp bases and are parallel-laminated (Fig. 8E), passing upward into very fine-grained ripple-bedded tops. Facies Association B contains finely comminuted plant detritus. Facies Association B crops out only in Location 1 and thins towards Location 2 (Figs 4 and 7).

Interpretation

Facies Association B was deposited by low velocity, unidirectional currents. The planar and current ripple lamination and siltstone interbeds indicate changes in velocity and sediment load. The fine-grained nature of FA B and the sharp bases of the sandstone elements may support an interpretation as crevasse splay deposits (Ethridge et al., 1981; Gersib & McCabe, 1981; Bridge, 1984) or crevasse subdeltas (Gugliotta et al., 2015). The presence of organic-rich mudstones interbedded with the sandstone and siltstone elements represent a local hiatus in crevasse splay deposition (e.g. Slingerland & Smith, 2004). No definitive terrestrial indicators, such as rootlets or palaeosols are observed in FA B, which may suggest that FA B represents subaqueous overbank deposition, perhaps in interdistributary bay areas (e.g. Elliott, 1974). However, the topset deposits of underlying clinothem units (for example, Cycle 2 of the Comaron Composite Sequence, see Dreyer et al., 1999), contain reddened floodplain palaeosols (Labourdette & Jones, 2007). A subaerial/subaqueous overbank interpretation is strengthened by the location of FA B within the geometric shelf-environment, suggesting a lower delta-plain environment.

Slope Deposits

Facies Association C: very fine-grained clean turbidites

Description (see Table 1)

Facies Association C (FA C) is predominantly composed of very fine-grained and fine-grained sandstone (44% and 47%, respectively, Fig. 7C) and has a mean grain size of 0.12 mm (very fine-grained sand; Fig. 6A). This FA is moderately well sorted (1.51 σ mean sorting; Fig. 6B). Grains are rounded to well-rounded and predominantly quartz. Facies Association C varies in thickness from 0.5 to 10.0 m, and individual beds are 0.05 to 0.4 m thick with a tabular appearance (Fig. 9A). Typically, bed bases are flat (Fig. 9A), although some are erosional, cutting up to 0.2 m deep into underlying siltstones. Typically, beds are ungraded, with local weak normal grading. The dominant sedimentary structures are current-ripple and plane-parallel lamination. Facies Association C has a 'clean' appearance, lacks observable plant detritus or organic matter, and is mica-poor (Fig. 9A). The very fine-grained sandstone beds are interbedded with bioclastic sandstone beds (0.5 to 2.0 m thick) dominated by Nummulites (Fig. 9B to D) (see Mateu-Vicens et al., 2012). In Location 2 (Figs 4 and 7), bioclastic sandstones are dominantly structureless (Fig. 9B), but in Locations 3 to 6 (Figs 4 and 7) they are normally graded (Fig. 9C); foraminifera are also found aligned parallel to internal laminations (Fig. 9D). Basinward, the mean grain-size of FA C varies slightly from 0.084 mm (very fine-grained sand) in Location 2, to 0.10 mm (very fine-grained sand) in Location 6

(Fig. 10A). Sorting shows an overall basinward decrease from 1.26 σ (very well sorted) in Location 2, to 1.59 σ (moderately well sorted) and 1.52 σ (moderately well sorted) in Locations 5 and 6, respectively (Fig. 10B). Facies Association C crops out from Location 2 to Location 6 (Fig. 7), showing an overall basinward-thinning. Facies Association C pinches out and terminates at Location 6, and shows no obvious vertical stratigraphic thickening or thinning trend.

Interpretation

The presence of both flat and erosive bed bases and abundant traction structures (including plane-parallel and current-ripple lamination) is consistent with deposition by turbidity currents (e.g. Lowe, 1982; Mutti et al., 2003; Hiscott et al., 1997; Plink-Björklund et al., 2001). The turbiditic nature of FA C is supported by its deposition on the geometric slope. The significant basinward thinning of FA C suggests deposition by gradual aggradation from decelerating turbidity currents (Kneller, 1995). The normal grading observed in FA C is also characteristic of waning turbidity currents (Bouma 1962, Walker 1967, Lowe 1982, Middleton 1993, Kneller 1995), which are deposited from transient, surge-type turbidity currents that progressively lose sediment carrying-capacity downslope (Lowe 1982, Hiscott 1994, Kneller & Branney 1995). These turbidites would be expected to show a basinward-fining trend (e.g. Lowe, 1982; Kneller, 1995; Mutti et al., 1999). However, the grain size of FA C shows minimal basinward change (<0.016 mm) from the zone of the clinoform rollover (Location 2) to the medial slope (Location 6) (Fig. 10A); this almost constant grain-size profile may reflect the original narrow grain-size range available for remobilisation and basinward transport. The 'clean' appearance of FA C (i.e. its negligible mica and terrestrial organic matter content), in combination with its high textural maturity (i.e. FA C is very fine-grained, well-sorted, well-rounded and quartz-rich) suggests sediment remobilisation from a wave-dominated shallow marine shelf deposit (e.g. Cosgrove et al., 2018). This is supported by the direct correlation of outer shelf to shelf-edge (Location 2) structureless foraminifera-bearing bioclastic sandstones with normally-graded bioclastic sandstones in the proximal and medial slope (Locations 3 to 6) (Figs 4 and 7). The structureless bioclastic sandstones represent *in situ* wave-dominated shallow-marine shelf deposits (Mateu-Vicens et al., 2012) and their basinward-equivalent, normally-graded bioclastic sandstones suggest the reworking and basinward transport of foraminifera-rich sands from the contemporaneous shelf.

Facies Association D: fine-grained micaceous turbidites

Description (see Table 1)

Facies Association D (FA D) is predominantly composed of very fine-grained and fine-grained sandstone (45% and 43%, respectively, Fig. 5D) with a mean grain size of 0.12 mm (very fine-grained sand; Fig. 6A). This FA is moderately well sorted (1.50 σ mean sorting; Fig. 6B). Facies Association D varies in thickness from 1.75 to 10.0 m (Fig. 7); individual beds are typically 0.4 to 2.5 m thick (Fig. 11A) and interbedded with 0.25 m thick siltstone beds (Fig. 11B). Typically, the base of FA D is erosional and contains abundant rip-up clasts (Fig. 11C). The FA D deposits typically thin and fine upward. Beds show normal, inverse and inverse to normal grading, and can be structureless, but most commonly display traction structures, including plane-parallel and current-ripple lamination (Fig. 11D). Facies Association D has a 'dirty' appearance, i.e. it has a high observable mica-content and contains finely comminuted plant detritus. Basinward, grain size shows a prominent fining trend, with mean grain diameter decreasing from 0.34 mm (medium-grained sand; Location 2) to 0.10 mm (very fine-grained sand; Location 7) (Fig. 10A). Sorting shows an overall downdip decrease from 1.35 σ (well-sorted; Location 2) to 1.5 σ (moderately well sorted; Location 7) (Fig. 10B). Facies Association D crops out from Location 2 to Location 7 (Figs 4 and 7). At Location 2, FA D can be correlated updip to the fluvial channel-fill associated with FA A. Facies Association D shows a marked basinward thinning trend (Fig. 7) and is commonly interbedded with FA C throughout the study area. Stratigraphically, FA D tends to thicken up-section.

Interpretation

The erosive bases of FA D, with aligned mudstone clasts and abundance of traction structures (including plane-parallel and current-ripple laminations) support an interpretation of deposition by turbidity currents (e.g. Lowe, 1982; Mutti et al., 2003; Hiscott et al., 1997; Plink-Björklund et al., 2001). The turbiditic nature of FA D is supported by its deposition on the geometric slope. The thick beds (up to 2.5 m) with traction structures are indicative of deposition from sustained turbidity currents, through gradual aggradation (Kneller, 1995). The significant thickness of individual turbidites may be indicative of deposition via hyperpycnal flows (e.g. Piper & Savoye, 1993; Mulder et al., 1998; Kneller & Buckee; 2000, Mulder & Alexander; 2001; Plink-Björklund & Steel; 2004), as river discharge can be sustained at a quasi-constant rate for hours, days or weeks (e.g. Wright et al., 1986; Hay, 1987; Prior et al., 1987; Wright et al., 1988; Nemec, 1990; Wright et al., 1990; Chikita, 1990; Zeng et al., 1991; Mulder et al., 1998; Piper et al., 1999). However, bed thickness cannot be used as a diagnostic criterion alone, as sustained flows can be triggered by various other mechanisms than river discharge (including volcanic eruptions, seismic activity and storm surges).

The physical connection from fluvial channel-fill (FA A) into slope deposits (FA D) suggests that the fluvial feeder system was directly depositing sediment onto the slope (e.g. Steel et al., 2000; Plink-Björklund et al., 2001; Plink-Björklund & Steel, 2002; Mellere et al., 2002; Plink-Björklund & Steel, 2004); this supports an interpretation of river-discharge-generated hyperpycnal flows that deposited their sediment load across the proximal to distal slope.

The presence of high amounts of plant debris and mica within FA D also supports a direct linkage between the fluvial and marine depositional environment (e.g. Mulder et al., 2003; Mutti et al., 2003; Plink-Björklund & Steel, 2004; Lamb et al., 2008; Zavala & Arcuri, 2016). Terrestrial organic matter and high concentrations of mica are widely used as indicators of hyperpycnal flows (e.g. Normark & Piper, 1991; Mulder & Syvitski, 1995; Mulder et al., 2003; Plink-Björklund & Steel, 2004; Zavala et al., 2011, 2012; Hodgson et al., 2018), associated with sustained river-derived flows during periods of high river discharge.

The basinward thinning and fining of FA D also supports deposition via hyperpycnal flows. As discussed in Plink-Björklund & Steel (2004), following flood termination coarser grain-size fractions are progressively deposited in a landward direction, and finer grain-size fractions are progressively deposited in a basinward direction, as flow velocity and sediment concentration decrease.

Repeated transitions between inverse and normal grading at intra-bed-scale, suggests the presence of accelerating (waxing) and decelerating (waning) flow regimes (cf. Kneller, 1995). As hyperpycnal flow beds are suggested to record variations in the flood hydrograph (e.g. Mulder & Alexander, 2001), the waxing episode of river-mouth discharge deposits an inversely graded division and a waning episode deposits a normally graded division, although these trends will not be present across an entire deposit (Mulder et al., 2001). However, inverse and normal grading at bed-scale may also reflect autogenic process, such as fluctuations in plunge-point position, which shred river discharge signals (Lamb et al., 2008, 2010).

Facies Association E: medium-grained, deformed turbidites

Description (see Table 1)

Facies Association E (FA E) is predominantly composed of medium-grained and coarse-grained sandstone (33% and 31%, respectively, Fig. 5E) and has a mean grain size of 0.39 mm (medium-grained

sand; Fig. 6A). This FA is moderately well-sorted (1.43 σ mean sorting; Fig. 6B). Facies Association E varies in thickness from 0.5 to 10.0 m; individual beds are 0.5 to 6.0 m thick (Fig. 12A). Bed-bases are commonly sharp and flat. However, erosional bed-bases are observed, cutting up to 0.3 m deep into underlying siltstone deposits; these surfaces are overlain directly by beds containing mudstone rip-up clasts. Beds show normal and inverse grading or may be ungraded. Facies Association E also shows extensive folding and 'ball and pillow' structures (Fig. 12B and C). Where deformation is less intense primary sedimentary structures are preserved including trough cross-stratification (Fig. 12D), parallel and ripple lamination and abundant internal amalgamation surfaces. Facies Association A has a 'dirty' appearance, and contains abundant finely comminuted plant detritus and is highly micaceous. Facies Association E exhibits a basinward coarsening trend from Locations 3 to 6 (Fig. 10A), where grain size increases from 0.33 mm (medium-grained sand) to 0.45 mm (medium grained sand); at Location 7, grain-size decreases to 0.31 (medium-grained sand). The basinward sorting trend of FA E across the sampled profile shows an initial increase from 1.5 σ (moderately well-sorted) to 1.3 σ (well-sorted) at Locations 3 and 4, respectively, and then decreases to 1.44 σ (moderately well-sorted) in Locations 6 and 7 (Fig. 10b). FA E crops out from Locations 2 to 7 (Figs 4 and 7) and can either thin in a basinward direction or remain at approximately the same thickness (Fig. 7). At Location 2, FA E cuts into and truncates FA A. Facies Association E is interbedded with FA C and FA D throughout the study area; FA E becomes thicker and more common up-section.

Interpretation

Erosional bases with aligned mudstone clasts, and the abundance of traction structures (including plane-parallel and ripple lamination) suggest deposition via turbidity currents (e.g. Lowe, 1982; Mutti et al., 2003; Hiscott et al., 1997; Plink-Björklund et al., 2001). The turbiditic nature of FA E is supported by its deposition on the geometric slope. The unidirectional cross-stratification suggests that current velocities were relatively high (Plink-Björklund et al., 2001). Trough cross-stratification is associated with migration of 3D dunes (Plink-Björklund et al., 2001; Stevenson et al., 2015; Hodgson et al., 2018). Similar to FA D, the significant thickness of individual turbidites (up to 6 m thick) may be indicative of deposition via hyperpycnal flows (e.g. Piper & Savoye, 1993; Mulder et al., 1998; Kneller & Buckee, 2000; Mulder & Alexander, 2001; Plink-Björklund & Steel, 2004; Tinterri, 2007). The presence of abundant terrestrial organic matter and high concentrations of mica might also support the interpretation of these deposits as hyperpycnites (e.g. Normark & Piper, 1991; Mulder & Syvitski, 1995; Mulder et al., 2003; Plink-Björklund & Steel, 2004; Zavala et al., 2011, 2012). Facies Association E shows repeated transitions

between inverse and normal grading at bed-scale (similarly to FA D, see above), suggesting the presence of accelerating (waxing) and decelerating (waning) flow regimes (cf. Kneller, 1995).

The folds and extensive contorted units indicate slope-induced deformation or slumping. The rapid deposition of sediment associated with hyperpycnal flows can lead to liquefaction processes, resulting in soft sediment deformation (e.g. Pontén & Plink-Björklund 2009; Plink-Björklund & Steel, 2004).

Unlike FA D, FA E deposits cannot be directly correlated updip to coeval fluvial channel-fill deposits (FA A), as FA E deposits start in the clinoform rollover zone (Location 2) and erodes into underlying fluvial channelized facies (FA A) (Fig. 7). This suggests strong bypass of the contemporaneous shelf and the active erosion and entrainment of underlying deposits, which may correspond with individual surges in river discharge (e.g. Talling, 2014). Additionally, the overall basinward-coarsening trend and general lack of obvious thinning suggests significant proximal bypass, flow acceleration (cf. Kneller et al., 1995) , and preferential sediment deposition in the medial and distal slope setting. The erosive nature of FA E and significant shelf-edge bypass suggests that flow velocity of FA E may have been higher, relative to FA D and supports a more catastrophic input of sediment associated with major river flooding events, rather than the sustained hyperpycnal flows associated with FA D.

Facies F: basinal mudstones

Description (see Table 1)

Facies Association F (FA F) is very fine- to fine-grained moderately sorted siltstone and varies significantly in thickness (0.5 m to 14.0 m). Typically, FA F is structureless or parallel-laminated, with 1 to 2 mm thick laminae. Bioturbation is highly variable in FA F (BI 0 to 4; see bioturbation index of Taylor & Goldring, 1993), but most commonly low (BI 1). Horizontal and vertical burrows are observed (60 mm long; 10 to 40 mm diameter). Facies Association F crops out across the complete depositional profile from Locations 1 to 7 (Figs 4 and 7) and becomes thicker in a basinward direction.

Interpretation

Facies Association F is interpreted to be the background sediment, accumulated mainly as a product of waning downslope-decelerating dilute turbidity currents (Kneller, 1995).

PROCESS-REGIME VARIABILITY

The distribution of slope facies within Cycle LG-1 shows the stratigraphic alternation between FA C, FA D and FA E. The sedimentary texture and structure of FA D and FA E suggest deposition under river-dominated shelf conditions. This is consistent with the interpretation of Dreyer et al. (1999) who interpreted the Sobrarbe Deltaic Complex overall to record a river-dominated system. However, the 'clean' and texturally mature nature of FA C is suggestive of a wave-dominated shelf process-regime. As such, this new dataset documents intra-clinothem process-regime variability, in which river-dominated conditions are episodically punctuated by wave-dominated conditions.

DOWNDIP CHANGES IN GRAIN SIZE AND SORTING

Grain size and sorting have been averaged for each sampling location to illustrate basin-scale changes in grain character (Figs 13 and 14). The grain-size variability in Cycle LG-1 is shown in Figs 13 and 14A. From Locations 1 to 3, there is a decrease in mean grain size from 0.46 mm (medium-grained sand; Location 1) to 0.21 mm (fine-grained sand; Location 3; Fig 14A). Location 1 has the highest inter-quartile grain-size variability (Fig. 14A). From Locations 4 to 7, mean grain size varies between sampling locations; mean grain-size is 0.25 mm (medium-grained sand), 0.10 mm (very fine-grained sand), 0.21 mm (fine-grained sand) and 0.18 mm (fine-grained sand) in Locations 4, 5, 6 and 7, respectively (Fig. 14A). The variation in sorting is illustrated by the box and whisker plots in Fig. 14B; it has a limited range from 1.4 (well-sorted, Location 1) to 1.58 (moderately well-sorted, Location 4), with a weak overall basinward decrease in sorting (Fig. 14B).

DISCUSSION

Mixed-process clinothem evolution

All clinothems within the Sobrarbe Deltaic Complex, including Cycle LG-1, have been previously interpreted to be 'river-dominated' (see Dreyer et al., 1999). However, detailed analysis of facies reveals a more complicated stratigraphic evolution of process-regime at an intra-clinothem scale. Changes in shelf process-regime result in prominent internal variability in sedimentary texture and structure across the complete depositional profile.

The documented process-regime change between river-dominated and wave-dominated affects the downdip geometric distribution of sedimentary bodies; in this case, sedimentary packages associated with a river-dominated process-regime (FA D and FA E), are distributed across the complete sampled

profile, from the shelf (topset) to the distal slope (foreset). In contrast, sand-dominated sedimentary packages associated with a wave-dominated process-regime (FA C), are deposited only in the proximal and medial slope environments. As such, distal slope deposits show prominent stratigraphic variability in grain-size; sand-rich packages are interbedded with >10 m silt-rich deposits. The termination, and downlap, of the wave-dominated, sand-facies on the medial slope results in the coeval deposition of silt in the lower slope setting. As such, only silt-grade sediment fractions are transported into the distal slope setting under a wave-dominated process-regime; intra-clinothem variability in shelf process-regime thus directly influences the architecture and sand-content of downdip deposits. The maximum basinward extent of FA C on the medial slope may reflect the maximum down-slope distance at which turbidity currents associated with coeval wave-dominated process regimes can transport their sand-fraction and illustrates their attenuated coarse-grained sediment transport capacity relative to turbidity currents associated with a river-dominated shelf.

Many clinothem systems are designated as being river-dominated, wave-dominated or tide-dominated (e.g. Dreyer et al., 1999; Pink-Björklund et al., 2001; Plink-Björklund & Steel, 2002; Deibert et al., 2003; Crabaugh & Steel, 2004; Plink-Björklund & Steel, 2004; Johannessen & Steel, 2005; Petter & Steel, 2006; Sylvester et al., 2012; Ryan et al., 2015). The use of end-member descriptors (i.e. river-dominated, wave-dominated or tide-dominated) has led to the under-recognition of mixed-energy clinothem systems in the ancient record (see Ainsworth et al., 2011; Olariu, 2014; Rossi & Steel, 2016). As such, relatively few ancient clinothems have been interpreted to document spatial and temporal variability in shelf (topset) process-regime (e.g. Ta et al., 2002; Ainsworth et al., 2008; Plink-Björklund, 2008; Carvajal & Steel, 2009; Vakarelov & Ainsworth, 2013; Jones et al., 2015; Gomis-Cartesio et al., 2017). Assigning a clinothem with a dominant shelf (topset) process-regime is also associated with discrete sedimentary processes and facies associations, which are used to inform archetypal river-dominated, wave-dominated or tide-dominated clinothem models (e.g. Elliott, 1986; Bhattacharya & Walker, 1992; Dalrymple, 1992; Walker & Plint, 1992). A traditional model of a prograding river-dominated clinothem is associated with a broadly coarsening-upward grain-size trends in shelf, slope and basin-floor deposits (Bhattacharya & Walker, 1992; Steel et al., 2008; Carvajal & Steel, 2009; Dixon et al., 2012b). However, as it is clearly documented in this case, applying an end-member shelf process-regime classification system to clinothem classification systems fails to adequately account for internal vertical and downdip variability in sedimentary texture associated with variability in topset process-regime conditions. This study highlights the internal textural variability of an individual clinothem, using detailed grain

characterisation, with potential implications for future studies of basin-margin successions. An additional factor to consider is lateral variability in shelf process regime, which will influence the along-strike distribution of facies and their associated grain character and stratigraphic thicknesses on the clinothem slope.

Sediment bypass at the clinoform rollover

In Cycle LG-1, the clinothem rollover (Locations 2 and 3) marks a prominent zone of grain-size fining (Figs 13 and 14A). Beyond the clinoform rollover zone, there is a basinward coarsening trend (Location 4), suggesting the presence of strongly bypassing flows across the shelf-edge. However, the bypass of coarse-grained sediment varies prominently between facies, according to: (i) the dominant process-regime in operation at the coeval shelf; and (ii) the hyperpycnal flow-style.

Turbidite beds of FA C (associated with wave-dominated shelf process-regime conditions), do not bypass coarse-grained sand downdip (Fig. 10A); in FA C grain size does not vary significantly at the clinoform rollover or along the depositional profile. The uniformity in grain size observed in FA C across the depositional profile reflects the well-sorted sediment source, possibly associated with previous reworking and winnowing processes at the shelf-edge under wave-dominated conditions (e.g. Roy et al., 1994; Bowman & Johnson, 2014; Cosgrove et al., 2018).

Although FA D and FA E are both associated with river-dominated shelf process-regimes, sediment bypass styles beyond the clinoform rollover vary between the two facies. This is attributed to their variable flow-styles. FA D (interpreted to represent sustained hyperpycnal flows) shows a general fining trend beyond the clinoform rollover and does not bypass large volumes of coarse-grained sand into the distal slope setting. The calibre of sand available at the river-mouth is likely to be a dominant factor controlling grain-size uniformity in FA D. Additionally, the lack of shelf incision associated with FA D indicates a low erosion and entrainment capacity, which attenuates the ability of sustained hyperpycnal flow deposits to incorporate coarser-grained sand-fractions from underlying deposits. In contrast, FA E bypasses the shelf setting and deposits coarse-grained sand in the medial and distal slope setting. The high-energy nature of the episodic hyperpycnal flows of FA E promotes bypass of the shelf and clinoform rollover (e.g. Petter & Steel, 2006), associated with erosion and entrainment of coarser-grained sand from underlying shelf deposits; this is evidenced by the incision of FA E into the underlying shelf deposits of FA A. In FA E, deposition of the coarsest sediment fractions occurs on the proximal and medial slope;

at the distal slope there is a decrease in mean grain size, associated with slope-gradient decrease and consequent flow deceleration (Figs 8 and 15).

In addition to influencing grain size across the depositional profile, the hyperpycnal flow type also influences the stratigraphic thicknesses of the resulting deposits. Episodic hyperpycnal flow deposits (FA E) are generally thicker, relative to their sustained hyperpycnal flow counterparts (FA D); this potentially implies that episodic hyperpycnal flows, associated with major flooding events, are able to transport and deposit higher sediment volumes relative to sustained hyperpycnal flows. However, this might seem counter-intuitive, as sustained hyperpycnal flows are likely to last longer and should thus result in greater stratigraphic bed-thicknesses compared to episodic hyperpycnal flows (e.g. Piper & Savoye; 1993; Mulder et al., 1998; Kneller & Buckee, 2000; Mulder & Alexander, 2001; Plink-Björklund & Steel, 2004). However, the relative thickness of FA E (episodic) relative to FA D (sustained) may be localised and represent an artefact of sampling along a 2D depositional profile. Additionally, this may imply that some of the sediment volume associated with FA D is bypassed further downslope into the basin-floor environment, which does not crop-out in this locality (Fig. 15).

Allogenic and autogenic process regime variability

Intra-clinothem process-regime variability may be driven by allogenic or autogenic forcings (e.g. Muto & Steel, 1997; Muto & Steel, 2014; Olariu, 2014). The duration of each cycle within the Sobrarbe Deltaic Complex is on the order of hundreds of thousands of years (Dreyer et al., 1999); as such within Cycle LG-1, intra-clinothem process regime variability occurred over timescales of tens of thousands of years. Allogenic variability, associated with small-scale relative sea-level variations, may account for the observed process-regime change in Cycle LG-1; this possibility is supported by the interpretations of Dreyer et al. (1999), who attribute intra-clinothem unconformities in the underlying Comaron composite sequences to high-frequency episodes of forced regression, associated with repeated small-scale tectonic tilting of the basin-floor. Variations in sediment supply rate provide an alternative allogenic cause of intra-clinothem process regime change. The river-dominated facies (FA D and FA E) may potentially be the result of climatically-activated river floods; as such, periods of heightened precipitation would have resulted in enhanced physical and chemical weathering, associated with increased terrestrial run-off (Schmitz, 1987; Peterson, et al., 2000). In contrast, wave-dominated facies (FA C) would be associated with periods of reduced sediment influx, associated with relatively drier climatic conditions. Variations in Eocene orbital cyclicity, related to the precessional (*ca* 25 kyr period

519 cycles) influence on precipitation patterns (e.g. Berger, 1978; Kutzbach & Otto-Bliesner, 1982), provide
520 another potential allogenic mechanism of regulating sediment transport over the timescales observed in
521 Cycle LG-1 (cf. Middle Eocene, Ainsa Basin; Cantalejo & Pickering, 2014).

522 Alternatively, autogenic processes such as river-channel avulsion, can result in a transient along-strike
523 shut-down of the direct connectivity between the river-dominated shelf and deep-water system.
524 Immediately downdip of the delta lobe switching and abandonment, a temporary shift to wave-
525 dominated conditions at the shelf-edge may occur. The case for an autogenic cause of process regime
526 variability is strengthened by the apparent rapidity (10 to 20 kyr) at which alternating river-dominated
527 and wave-dominated conditions are recorded in the stratigraphic record (e.g. Amorosi & Milli, 2001;
528 Amorosi et al., 2003; 2005; Correggiari et al., 2005; Olariu, 2014).

529 Both allogenic and autogenic drivers of process regime change are plausible for Cycle LG-1 and are
530 difficult to distinguish in the absence of additional strike-parallel exposure. However, based on the
531 abrupt intra-clinothem facies changes, and the localised preservation of wave-dominated facies (i.e.
532 wave-dominated conditions are not documented at intra-clinothem scales in other minor sequences;
533 Dreyer et al., 1999), autogenic river-avulsion is the favoured mechanism of intra-clinothem process
534 regime variability in this case.

535 CONCLUSIONS

536 This study integrates quantitative analysis of grain size and sorting with a traditional outcrop-based
537 study of a single topset-to-bottomset clinothem within the Las Gorgas composite sequence of the
538 Eocene Sobrarbe Deltaic Complex. In the oldest clinothem of the Las Gorgas composite sequence
539 (named here Cycle LG-1), five sandstone-dominated facies have been identified, based on sedimentary
540 texture and structure, and bed geometry. The sandstone-dominated facies associations show
541 quantitative differences in grain size and sorting. Slope deposits are dominated by organic-rich and
542 micaceous hyperpycnal flow deposits (Facies Association D and Facies Association E); these are
543 associated with coeval river-dominated topset deposits (Facies Association A and Facies Association B).
544 Two depositional styles are observed in FA D and FA E, related to the nature of the hyperpycnal flooding
545 events: sustained (FA D), versus episodic (FA E). Sustained hyperpycnal flow deposits show direct river
546 connectivity between the outer-shelf and proximal slope and result in the deposition of fine-grained
547 sand across the complete depositional profile. Episodic hyperpycnal flows mostly bypass the clinoform

548 rollover and incise underlying shelf deposits; deposition of medium-grained and coarse-grained sand
549 occurs mostly on the proximal to distal slope. Episodic flows are interpreted to have higher flux rates,
550 and ultimately may transport more sediment into distal slope settings than lower flux rate sustained
551 flows of longer duration.

552 Hyperpycnal-flow deposits are interbedded with much cleaner (terrestrial organic matter-poor and
553 mica-poor), finer-grained turbidites (FA C), which do not show characteristics consistent with their
554 hyperpycnal counterparts. The clean and relatively fine-grained nature of FA C suggests strong
555 reworking or deposition under a wave-dominated process regime, under which clean shelf-edge sands
556 are remobilised as turbidity currents. The wave-dominated regime deposits are entirely absent from the
557 distal slope. The facies distributions documented in Cycle LG-1 are therefore the result of rapid temporal
558 changes in the dominant process regime, occurring over timescales of tens of thousands of years; these
559 transitions are interpreted to be the result of autogenic variability at an intra-clinothem scale, and
560 mostly associated with river-avulsion processes.

561 Quantitatively-documented basinward changes in grain size, alongside facies distributions, indicate that
562 coarse-grained sediment bypass at the clinoform rollover varies according to both the dominant
563 process-regime in operation at the shelf-edge (i.e. wave-dominated versus river-dominated) and the
564 flow-style of river-dominated deposits (i.e. sustained versus episodic hyperpycnal flows). In Cycle LG-1,
565 bypass into the deeper-water setting is driven by episodic hyperpycnal flows; sustained hyperpycnal
566 flows and turbidity currents associated with a wave-dominated shelf do not bypass coarse-grained
567 sediment downdip. Instead, all grain sizes are deposited across the slope setting, facilitating clinoform
568 progradation. As such, heterogeneity in grain size is documented not only at a process-regime scale, but
569 variability in coarse-grained sand bypass can be introduced based on the dominant flow-style.

570 This study applies integrated quantitative grain size and sorting data and sedimentology in order
571 understand the evolution of an individual clinothem sequence. This novel dataset highlights hitherto
572 undocumented intra-clinothem variability, which is directly related to changes in the shelf process-
573 regime. Updip shelf process-regime is a fundamental factor controlling downdip architecture and
574 sedimentary texture. The outcrop example from Cycle LG-1, also highlights the complexity and
575 heterogeneity of different flow-types, such that flows associated with sustained and episodic
576 hyperpycnal flows also modulate the distribution, calibre and maturity of sediment transported

downdip. This novel outcrop-based study of grain character may be used as a predictive reference for subsurface exploration and provides new insights into the evolution of individual clinothem sequences.

ACKNOWLEDGEMENTS

We would like to thank the John Wyn-Williams and the Leeds Electron Microscopy and Spectroscopy Centre for their assistance with the preparation and imaging of samples, respectively. We would also like to thank the Institute of Applied Geoscience at the University of Leeds for financial assistance, and Grace and Finn Hodgson for assistance with UAV data collection. We thank reviewers Piret Plink-Björklund and Roberto Tinterri, and Associate Editor Massimiliano Ghinassi for their valuable comments and advice, which have significantly improved this manuscript.

REFERENCES

Adams, E.W. and Schlager, W. (2000) Basic types of submarine slope curvature. *J. Sed. Res*., **70**, 814-828.

Ainsworth, R.B., Vakarelov, B.K., and Nanson, R.A. (2011) Dynamic spatial and temporal prediction of changes in depositional processes on clastic shorelines: toward improved subsurface uncertainty reduction and management. *AAPG Bull.*, **95**, 267-297.

Ainsworth, R. B., Flint, S.S., and Howell, J.A. (2008) Predicting coastal depositional style: Influence of basin morphology and accommodation to sediment supply ratio within a sequence-stratigraphic framework. In*: Recent advances in models of shallow-marine stratigraphy* (Eds G.J. Hampson, R.J. Steel, P.M. Burgess, R.W. Dalrymple), *SEPM Spec. Publ.*, 90, 237-263.

Amorosi, A. and Milli, S. (2001) Late Quaternary depositional architecture of Po and Tevere river deltas (Italy) and worldwide comparison with coeval deltaic successions. *Sed. Geol*. **144**, 357-375.

Amorosi, A., Centineo, M. C., Colalongo, M. L., Pasini, G., Sarti, G. and Vaiani, S. C. (2003) Facies architecture and latest Pleistocene–Holocene depositional history of the Po Delta (Comacchio area), Italy. *J. Geol.* **111**, 39-56.

Amorosi, A., Centineo, M. C., Colalongo, M. L. and Fiorini, F. (2005) Millennial-scale depositional cycles from the Holocene of the Po Plain, Italy. *Mar. Geol*., **222**, 7-18.

Anell, I. and Midtkandal, I. (2015) The quantifiable clinothem - types, shapes and geometric relationships in the Plio-Pleistocene Giant Foresets Formation, Taranaki Basin, New Zealand. *Basin Res*. **29**, 277-297.

Asquith, D.O. (1970) Depositional topography and major marine environments, Late Cretaceous, Wyoming. *AAPG Bul.* **54**, 1184–1224.

Berger, A. (1978) Long-term variations of caloric insolation resulting from the Earth's orbital parameters. *Quatern. Res.* **9**, 139-167.

Bhattacharya, J.P. (2006), Deltas. In*: Facies Models Revisited* (Eds R.G. Walker, and H. Posamentier, H.), *SEPM Spec. Publ.*, 84, 237-292.

Bhattacharya, J. P. and Walker, R.G. (1992) Deltas. In: *Facies Models; Response to Sea Level Change* (Eds R.G. Walker and N.P. James), Geol. Assoc. Can. 157–177 pp.

Blott, S.J. and Pye, K. (2001) GRADISTAT: a grain-size distribution and statistics package for the analysis of unconsolidated sediments. *Earth Surf. Proc. Land*. **26**, 1237-1248.

Bouma, A.H. (1962) Sedimentology of Some Flysch Deposits: A Graphic Approach to Facies Interpretation. Elsevier, Amsterdam. 168.

Bowman, A.P. and Johnson, H.D. (2014) Storm-dominated shelf-edge delta successions in a high accommodation setting: The palaeo-Orinoco Delta (Mayaro Formation), Columbus Basin, South-East Trinidad. *Sedimentology,* **61**, 792-835.

Bridge, J.S. (1984) Large-scale facies sequences in alluvial overbank environments. *J. Sed. Res.,* **54**, 85-170.

Bridge, J. S., Smith, N.D., Trent, F., Gabel, S. L. and Bernstein, P. (1986) Sedimentology and morphology of a low-sinuosity river: Calamus River, Nebraska Sand Hills. *Sedimentology*, **33**, 851–870.

Brunet, M.F. (1986) The influence of the Pyrenees on the development of the adjacent basin. *Tectonophysics*, **129**, 343-354.

Cantalejo, B. and Pickering, K.P. (2014) Climate forcing of fine-grained deep-marine systems in an active tectonic setting: Middle Eocene, Ainsa Basin, Spanish Pyrenees. *Palaeogeogr. Palaeoclimatol. Palaeoecol.,* **410**, 351-371.

Carvajal, C. and Steel, R. (2006) Thick turbidite successions from supply-dominated shelves during sea-level highstand. *Geology*, **34**, 665-668.

Carvajal, C. and Steel, R. (2009) Shelf-edge architecture and bypass of sand to deep water: influence of shelf-edge processes, sea level and sediment supply. *J. Sed. Res.,* **79**, 652-672.

Catuneanu, O., Abreu, V., Bhattacharya, J.P., Blum, M.D., Dalrymple, R.W., Eriksson, P.G., Fielding, C.R., Fisher, W.L., Galloway, W.E., Gibling, M.R., Giles, K.A., Holbrook, K.A., Jordon, J.M., Kendall, R., Macurda, C.G. St., Macurda, C.B., Martinsen, O.J., Miall, A.D., Neal, J.E., Nummendal, D., Pomar, L., Posamentier, H.W., Pratt, B.R., Sarg, J.F., Shanley, K.W., Steel, R.J., Strasser, A. and Tucker, M.E.C. (2009) Towards the standardization of sequence stratigraphy. *Earth-Sci. Rev.,* **92**, 1-33.

Chayes, F. (1950) On the bias of grain-size measurements made in thin-section. *J. Geol.,* **58**, 156-160.

639 Chikita, K. (1990) Sedimentation by river-induced turbidity currents: field measurements and
640 interpretation. *Sedimentology*, **37**, 891-905.

641 Collinson, J.D., Mountney, N. P. and Thompson, D. B. (2006) Sedimentary Structures. 3rd edn, Terra
642 Publishing, Harpenden, 292 pp.

643 Correggiari, A., Cattaneo, A. and Trincardi, F. (2005) The modern Po Delta system: lobe switching and
644 asymmetric prodelta growth. *Mar. Geol.,* **222**, 49-74.

645 Cosgrove, G. I., Hodgson, D. M., Poyatos-Moré, M., Mountney, N. P. and McCaffrey, W. D. (2018). Filter
646 or conveyor? Establishing relationships between clinoform rollover trajectory, sedimentary process
647 regime, and grain Character within intrashelf clinothems, Offshore New Jersey, USA. *J. Sed. Res.,* **88**,
648 917-941.
649
650 Cosgrove, G.I.E., Hodgson, D.M., M., Mountney, N.P., McCaffrey, W.M.D., 2019, High-resolution
651 correlations of strata within a sand-rich sequence clinothem using grain fabric data, offshore New
652 Jersey, USA. *Geosphere,* **19,** https://doi.org/10.1130/GES02046.1.

653 Crabaugh, J.P. and Steel, R.J. (2004) Basin-floor fans of the Central Tertiary Basin, Spitsbergen:
654 relationship of basin-floor sand-bodies to prograding clinoforms in a structurally active basin. *Geol. Soc.*
655 *London Spec. Pub.,* 222, 187-208.
656
657 Dalrymple, R.W. (1992) Tidal depositional systems. In: *Facies Models: Response to Sea-Level Change*
658 (Eds. R.G., Walker and N.P., James). *Geol. Assoc. Canada*, p. 195–218.

659 DeFrederico, A. (1981) La sedimentacion de talud en el sector occidental de la cuenca Paleogena de
660 Ainsa, Autonoma de Barcelona, Publicaciones de Geolocationia, 270 pp.
661
662 Deibert, J.E., Benda, T., Løseth, T., Schellpeper, M. and Steel, R.J. (2003) Eocene clinoform growth in
663 front of a storm-wave-dominated shelf, Central Basin, Spitsbergen: No significant sand delivery to
664 deepwater area. *J. Sed. Res.,* **23**, 546-558.

665 Dixon, J.F., Steel, R.J. and Olariu, C. (2012a) River-dominated shelf-edge deltas: delivery of sand across
666 the shelf break in the absence of slope incision. *Sedimentology*, **59**, 1133-1157.

667 Dixon, J.F., Steel, R.J. and Olariu, C. (2012b) Shelf-edge delta regime as a predictor of the deep-water
668 deposition. *J. Sed. Res.,* **82**, 681-687.

669 Donovan, A. (2003) Depositional topography and sequence development. In: *Shelf margin deltas and*
670 *linked down slope petroleum systems: Global significance and future exploration potential* (Eds. H.H.
671 Roberts, N.C. Rosen, R.H. Fillon and J.B. Anderson). *GCSSEPM Spec. Publ.*, 23, 493-522.

672 Dreyer, T., Corregidor, J., Arbues, P. and Puigdefabregas, C. (1999) Architecture of the tectonically
673 influenced Sobrarbe deltaic complex in the Ainsa Basin, northern Spain. *Sed. Geol.,* **127**, 127-169.
674 Elliott, T. (1986) Deltas. In: *Sedimentary Environments and Facies* (Eds. H.G. Reading), Oxford, U.K.,
675 Blackwell Scientific Publications, p. 113–154.
676 Elliott, T. (1974) Interdistributary bay sequences and their genesis. *Sedimentology,* **21**, 611-622.

677 Ethridge, F.G., Jackson, T.J. and Youngberg, A.D. (1981) Floodbasin sequence of a fine-grained meander
678 belt subsystem: The coal-bearing Lower Wasatch and Upper Fort Union Formations, Southern Powder
679 River Basin, Wyoming. In: *Recent and Ancient Nonmarine Depositional Environments* (Eds F.G. Ethridge),
680 *SEPM Spec. Publ.,* 31, 191-209

681 Farrell, K.M. (1987) Sedimentology and facies architecture of overbank deposits of the Mississippi River,
682 False River region, Louisiana. In: *Recent Developments in Fluvial Sedimentology* (Eds F.G. Ethridge and
683 R.M. Flores), *SEPM Spec. Publ.,* 39, 111-120.

684 Fernández, O., Muñoz, J.A., Arbues, P. and Marzo, M. (2004) Three dimensional reconstruction of
685 Geological surfaces: An example of growth strata and turbidite systems from the Ainsa Basin (Pyrenees,
686 Spain). *AAPG Bull.,* **88**, 1049-1068.

687 Galloway, W.E. (1989) Genetic stratigraphic sequences in basin analysis 1: architecture and genesis of
688 flooding-surface bounded depositional units. *AAPG Bull.,* **73**, 125-142.

689 Gammon, P.R., Neville, L.A., Patterson, R.T., Savard, M.M. and Swindles, G.T. (2017) A log-normal
690 spectral analysis of inorganic grain-size distributions from a Canadian boreal lake core: Towards refining
691 depositional process proxy data from high latitude lakes. *Sedimentology*, **64**, 609-630.

692 Gersib, G.A. and McCabe, P.J. (1981) Continental coal-bearing sediments of the Port Hood Formation
693 (Carboniferous), Cape Linzee, Nova Scotia, Canada. *SEPM Spec. Publ.,* **31**, 95-108.

694 Gilbert, G.K. (1885) The topographic feature of lake shores. U.S. Geol. Surv. Annual Report, **5**, 104 -108.

695 Glørstad-Clark, E., Faleide, J.I., Lundschien, B.A. and Nystuen, J.P. (2010) Triassic seismic sequence
696 stratigraphy and paleogeography of the Western Barents Sea area. *Mar. Petrol. Geol.,* **27**, 1448-1475.

697 Glørstad-Clark, E., Birkeland, E.P., Nystuen, J.P., Faleide, J.I. and Midtkandal, I. (2011) Triassic platform-
698 margin deltas in the Western Barents Sea. *Mar. Petrol. Geol.,* **28**, 1294-1314.

699 Gomis-Cartesio, L.E., Poyatos-Moré, M., Flint, S.S., Hodgson, D.M., Brunt, R.L. and Wickens, H.D.V.
700 (2017) Anatomy of a mixed-influence shelf edge delta, Karoo Basin, South Africa. In: *Sedimentology of*
701 *Paralic Reservoirs: Recent Advances* (Eds G.J. Hampson, A.D. Reynolds, B. Kostic and M.R. Wells). *Geol.*
702 *Soc. London Spec. Publ.,* 444, 393-418.

703 Greenman, N.N. (1951) On the bias of grain-size measurements made in thin-section: a discussion. *J.*
704 *Geol.,* **59**, 268-274.

705 Gugliotta, M., Flint, S.S., Hodgson, D.M. and Veiga, G.D. (2015) Stratigraphic record of river-dominated
706 crevasse subdeltas with tidal influence (Lajas Formation, Argentina). *J. Sed. Res.*, **85**, 265-284.

707 Hadler-Jacobsen, F., Johannessen, E.P., Ashton, N., Henriksen, S., Johnson, S.D. and Kristensen, J.B.
708 (2005) Submarine fan morphology and lithology distribution: a predictable function of sediment
709 delivery, gross shelf-to-basin relief, slope gradient and basin topography. In: *Petroleum Geology: North-*
710 *west Europe and Global Perspectives* (Eds A.G. Dore, and B.A. Vinin), *Proceedings of the 6th Petroleum*
711 *Geology Conference Geol. Soc. London,* 1121-1145.

712 Hay, A.E. (1987) Turbidity currents and submarine channel formation in Rupert Inlet, British Columbia:
713 The roles of continuous and surge-type flow. *J. Geophys. Res.* **92**, 2883-2900.

714 Helland-Hansen, W. (1992) Geometry and facies of Tertiary clinothems, Spitsbergen. *Sedimentology*, **39**,
715 1013-1029.

716 Helland-Hansen, W. and Hampson, G.J. (2009) Trajectory analysis: concepts and applications. *Basin Res.,*
717 **21**, 454-483.

718 Henriksen, S., Hampson, G.J., Helland-Hansen, W., Johannessen, E.P. and Steel, R.J. (2009) Shelf edge
719 and shoreline trajectories, a dynamic approach to stratigraphic analysis. *Basin Res*., **21**, 445-453.

Hiscott, R.N. (1994) Loss of capacity, not competence, as the fundamental process governing deposition from turbidity currents. *J. Sed. Res.*, **64**, 209-214.

Hiscott, R.N., Pickering, K.T., Bouma, A.H., Hand, B.M., Kneller, B.C., Postma, G. and Soh, W. (1997) Basin-floor fans in the North Sea: sequence stratigraphic models vs. sedimentary Facies: discussion. *AAPG Bull.,* **81**, 662-665.

Hodgson, D.M., Browning, J.V., Miller, K.G., Hesselbo, S., Poyatos-Moré, Mountain, G.S. and Proust, J.-N. (2018) Sedimentology, stratigraphic context, and implications of Miocene bottomset deposits, offshore New Jersey. *Geosphere*, **14**, 95-114.

Hubbard, S.M., Fildani, A., Romans, B.W., Covault, J.A. and McHargue, T.R. (2010) High-relief slope clinoform development: insights from outcrop, Magallanes Basin, Chile. *J. Sed. Res.,* **80**, 357-375.

Jennette, D.C., Wawrzyniec, T., Fouad, D., Dunlap, D., Munoz, R., Barrera, D., Williams-Rojas, C. and Escamilla-Herra, A. (2003) Traps and turbidite reservoir characteristics from a complex and evolving tectonic setting, Veracrus Basin, southeastern Mexico. *AAPG Bull.,* **87**, 1599-1622.

Johannessen, E.P. and Steel, R.J. (2005) Shelf-margin clinoforms and prediction of deepwater sands. *Basin Res.,* **17**, 521-550.

Jones, G.E.D., Hodgson, D.M. and Flint, S.S. (2013) Contrast in the process response of stacked clinothems to the shelf-slope rollover. *Geosphere*, **9**, 299-316.

Jones, G.E.D., Hodgson, D.M. and Flint, S.S. (2015) Lateral variability in clinoform trajectory, process regime, and sediment dispersal patterns beyond the shelf-edge roll over in exhumed basin margin-scale clinothems. *Basin Res.,* **27**, 657-680.

Kellerhals, R., Shaw, J. and Arora, V.K. (1975) On grain size from thin sections. *J. Geol.,* **83**, 79-86.

Kneller, B., (1995) Beyond the turbidite paradigm: physical models for deposition of turbidites and their implications for reservoir prediction. In: Characterization of Deep Marine Clastic Systems (Eds. A.J., Hartley and D.J. Prosser), *Geol. Soc. Spec. Publ.,* 94, 31–49.

Kneller, B.C. and Branney, M.J. (1995) Sustained high-density turbidity currents and the deposition of thick ungraded sands. *Sedimentology*, **42**, 607-616.

Kneller, B. and Buckee, C. (2000) The structure and fluid mechanics of turbidity currents: a review of some recent studies and their geological implications. *Sedimentology*, **47,** 62-94.

Kutzbach, J.E. and Otto-Bliesner, B.L. (1982) The sensitivity of the African-Asian monsoonal climate to orbital parameter changes for 9000 years BP in a low-resolution general circulation model. *J. Atmos. Sci,* **39**, 1177-1188.

Labourdette, R. and Jones, R.R. (2007) Characterization of fluvial architectural elements using a three-dimensional outcrop data set: Escanilla braided system, South-Central Pyrenees, Spain. *Geosphere,* **3**, 422-434.

Lamb, M.P., Myrow, P.M., Lukens, C., Houck, K. and Strauss, J. (2008) Deposits from wave-influenced turbidity currents: Pennsylvanian Minturn Formation, Colorado, USA. *J. Sed. Res.,* **78**, 480-498.

Lamb, M.P., McElroy, B., Kopriva, B., Shaw, J. and Mohrig, D. (2010) Linking river-flood dynamics to hyperpycnal-plume deposits: Experiments, theory, and geological implications. *GSA Bull.,* **122**, 1389-1400.

Laugier, F.J. and Plink-Björklund, P. (2016) Defining the shelf edge and the three-dimensional shelf edge to slope facies variability in shelf-edge deltas. *Sedimentology*, **63**, 1280-1320.

Lowe, D.R. (1982) Sediment gravity flows: II. Depositional models with special reference to the deposits of high-density turbidity currents. *J. Sed. Petrol.,* **52**, 279-297.

Mateu-Vicens, G., Pomar, L. and Ferràndez-Cañadell, C. (2011) Nummulitic banks in the upper Lutetian 'Buil level', Ainsa Basin, South Central Pyrenean Zone: the impact of internal waves. *Sedimentology*, **59**, 527-552.

Mellere, D., Plink-Björklund, P. and Steel, R. (2002) Anatomy of shelf deltas at the edge of a prograding Eocene shelf margin, Spitsbergen. *Sedimentology*, **49**, 1181-1206.

Middleton, G.V. (1993) Sediment deposition from turbidity currents. *Annu. Rev. Earth Planet. Sci.,* **21**, 89-114.

Mitchum, R.M., Vail, P.R. and Thompson, S. (1977) Seismic stratigraphy and global changes in sea level, part 2: the depositional sequence as the basic unit for stratigraphic analysis. In: *Seismic Stratigraphy: Applications to Hydrocarbon Exploration* (Ed C.E. Payton). *AAPG Mem.,* **26**, 53-62.

Muñoz, J.A. (1992) Evolution of a continental collision belt: ECORS-Pyrenees crustal balanced cross-section. In: Thrust Tectonics (Ed K.R. McClay) Chapman and Hall, London, 235-246 pp.

Muñoz, J.A., Arbues, P. and Serra-Kiel, J. (1998) The Ainsa Basin and the Sobrarbe oblique thrust system: sedimentological and tectonic processes controlling slope and platform sequences deposited synchronously with a submarine emergent thrust system. In: Field Trip Guidebook of the 15th International Sedimentological Congress, Alicante (Eds. A.M. Hevia and A.R. Soria), 213–223.

Mulder, T. and Alexander, J. (2001) The physical character of subaqueous sedimentary density flows and their deposits. *Sedimentology*, **48**, 269-299.

Mulder, T. and Syvitski, J.P.M. (1995) Turbidity current generated at river mouths during exceptional discharges to the world oceans. *J. Geol.,* **103**, 285–299.

Mulder, T., Migeon, S., Savoye, B. and Faugéres, J.-C. (2001) Inversely graded turbidite sequences in the deep Mediterranean. A record of deposits from flood-generated turbidity currents? *Geo-Mar. Letters,* **21**, 86–93.

Mulder, T., Syvitski, J.P.M., Migeon, S., Faugéres, J-C. and Savoye, B. (2003) Marine hyperpycnal flows: initiation, behaviour and related deposits. A review. *Mar. Petrol. Geol.,* **20**, 861-882.

Mulder, T., Syvitski, J.P.M. and Skene, K.I. (1998) Modeling erosion and deposition by turbidity currents generated at river mouths. *J. Sed. Res.,* **68**, 124-137.

Muto, T. and Steel, R.J. (1997) Principles of regression and transgression: the nature of the interplay between accommodation and sediment supply. *J. Sed. Res.,* **67**, 994–1000.

Muto, T. and Steel, R.J. (2014) The autostratigraphic view of responses of river deltas to external forcing: Development of the concept. *Int. Assoc. Sedimentol. Spec. Publ.,* 47, 139-148.

794 Mutti, E., Tinterri, R., Remacha, E., Mavilla, N., Angella, S. and Fava, L. (1999) An Introduction to the
795 analysis of ancient turbidite basins from an outcrop perspective. *AAPG Continuing Education Course*
796 *Note Series*, 39, 61 p.

797 Mutti, E., Steffens, G.S., Pirmez, C., Orlando, M. and Roberts, D. (2003) Turbidites: Models and Problems:
798 *Mar. Pet. Geol.,* **20**, 523-933.Nemec, W. (1990) Aspects of sediment movement on steep delta slopes. In:
799 *Coarse-Grained Deltas* (Eds A. Colella and D.B. Prior), *Int. Assoc. Sedimentol. Spec. Publ.,* 10, 29 – 73.

800 Normark, W.R. and Piper, D.J. (1991) Initiation processes and flow evolution of turbidity currents:
801 implications for the depositional record. *SEPM Spec. Publ.,* 46, 207–230.

802 Olariu, C. (2014) Autogenic process change in modern deltas: lessons from the ancient. In: *From*
803 *Depositional Systems to Sedimentary Successions on the Norwegian Continental Margin* (Eds A.W.
804 Martinius, R. Ravnås, J.A. Howell, R.J. Steel and J.P. Wonham, J.P.). *Int. Assoc. Sedimentol. Spec. Publ.,*
805 46, 149-166.

806 Patruno, S., Hampson, G.J. and Jackson C, A-L. (2015) Quantitative characterisation of deltaic and
807 subaqueous clinoforms. *Earth Sci. Rev.,* **142**, 79-119.

808 Patruno, S. and Helland-Hansen, W. (2018) Clinoforms and clinoform systems: Review and dynamic
809 classification scheme for shorelines, subaqueous deltas, shelf edges and continental margins. *Earth Sci.*
810 *Rev.,* **185**, 202-233.

811 Peterson, L.C., Haug, G.H., Hughen, K.A., Rohl, U. (2000) Rapid changes in the hydrologic cycle of the
812 Tropical Atlantic during the last glacial. *Science*, **290**, 1947-1951.

813 Petter, A.L. and Steel, R.J. (2006) Hyperpycnal flow variability and slope organization on an Eocene shelf
814 margin, central basin, Spitsbergen. *AAPG Bull.,* 90, 1451-1472.

815 Pinous, O.V., Levchuck, M.A. and Sahagian, D.L. (2001) Regional synthesis of the productive Neocomian
816 complex of West Siberia: sequence stratigraphic framework. *AAPG Bull.,* 85, 1713-1730.

817 Piper, D.J.W. and Savoye, B. (1993) Processes of late Quaternary turbidity current flow and deposition
818 on the Var fan, north-west Mediterranean Sea. *Sedimentology,* **40**, 557-582.

819 Piper, D.J.W., Hiscott, R.N. and Normark, W.R. (1999) Outcrop-scale acoustic facies analysis and latest
820 Quaternary development of Hueneme and Dume submarine fans, offshore California. *Sedimentology*,
821 **46**, 47-78.

822 Pirmez, C., Pratson, L.F. and Steckler, M.S. (1998) Clinoform development by advection–diffusion of
823 suspended sediment: modeling and comparison to natural systems. *J. Geophys. Res*., **103**, 141-157.

824 Plink-Björklund, P. (2008) Wave-to-tide process change in a Campanian shoreline complex, Chimney
825 Rock Tongue, Wyoming and Utah. In: *Recent Advances in Models of Siliciclastic Shallow-Marine*
826 *Stratigraphy* (Eds G.J. Hampson, R.J. Steel, P.M. Burgess and R.W. Dalrymple), *SEPM Spec. Publ*., 90,
827 265–291.

828 Plink-Björklund, P., Mellere, D. and Steel, R. (2001) Turbidite variability and architecture of sand-prone,
829 deep-water slopes: Eocene clinoforms in the Central Basin, Spitsbergen. *J. Sed. Res.,* **71**, 895-912.

830 Plink-Björklund, P. and Steel, R.J. (2002) Perched-delta architecture and the detection of sea level fall
831 and rise in a slope-turbidite accumulation, Eocene Spitsbergen. *Geology*, **30**, 115–118.

832 Plink-Björklund, P. and Steel, R.J. (2004) Initiation of turbidity currents: outcrop evidence for Eocene
833 hyperpycnal flow turbidites. *Sed. Geol.,* **165**, 29–52.

834 Poblet, J., Muñoz, J.A., Yrave, A. and Serra-Kiel, J. (1998) Quantifying the kinematics of detachment folds
835 using three-dimensional geometry: Application to the Mediano anticline (Pyrenees, Spain). *Geol. Soc.*
836 *Am. Bull.,* **110**, 111-125.

837 Pontén, A. and Plink-Bjorklund, P. (2009) Process regime changes across a regressive to transgressive
838 turnaround in a shelf-slope basin, Eocene central basin of Spitsbergen. *J. Sed. Res.,* **79**, 2-23.

839 Poyatos-Moré, M., Jones, G.D., Brunt, R.L., Tek, D., Hodgson, D.M. and Flint, S.S. (2019) Clinoform
840 architecture and facies distribution through an erosional to accretionary basin margin transition. *Basin*
841 *Res.* In Press: https://doi.org/10.1111/bre.12351

842 Prior, D.B., Bornhold, B.D, Wiseman Jr., W.J. and Lowe, D.R. (1987) Turbidity current activity in a British
843 Columbia fjord. *Science,* **237**, 581-584.

844 Puigdefàbregas, C. (1975) La sedimentacion molasica en la Cuenca de Jaca. *Monografia del Instituto de*
845 *Estudios Pirineos*, **104**, 1-88.

846 Pyles, D.R. and Slatt, R.M. (2007) Stratigraphic evolution of the Upper Cretaceous Lewis Shale, Southern
847 Wyoming: Applications to understanding shelf to base-of-slope changes in stratigraphic architecture of
848 mud-dominated, progradational depositional systems. In: *Atlas of Deepwater Outcrops* (Eds T.H. Nilsen,
849 R.D. Shew, G.S. Steffebd, J.R.J. Studlick). AAPG Stud. Geol., **56**, 19.

850 Rich, J.L. (1951) Three critical environments of deposition and criteria for recognition of rocks deposited
851 in each of them. *Geol. Soc. Am. Bull.,* **62**, 1-20.

852 Ross, W.C., Watts, D.E. and May, J.A. (1995) Insights from stratigraphic modelling: mud-limited versus
853 sand-limited depositional systems. *AAPG Bull.*, **79**, 231-258.

854 Rossi, V.M. and Steel, R.J. (2016) The role of tidal, wave and river currents in the evolution of mixed-
855 energy deltas: example from the Lajas Formation (Argentina). *Sedimentology,* **63**, 824-864.

856 Roy, P.S., Cowell, P.J., Ferland, M.A. and Thom, B.G. (1994) Wave-dominated coasts. In: Coastal
857 Evolution: Late Quaternary Shoreline Morphodynamics (Eds R.W.G. Carter and C.D. Woodroffe),
858 Cambridge, UK, Cambridge University Press, 121 pp.

859 Schmitz, B. (1987) The TiO_2/Al_2O_3 ratio in the Cenozoic Bengal Abyssal Fan sediments and its use as a
860 paleostream indicator. *Mar. Geol.,* **76**, 195-206.

861 Slingerland, R. and Smith, N.D. (2004) River avulsions and their deposits. *Ann. Rev. Earth Plan. Sci*., **32**,
862 257–285.

863 St-Onge, G., Mulder, T., Piper, D.J.W., Hillaire-Marcel, C. and Stoner, J.S. (2004) Earthquake and flood-
864 induced turbidites in the Saguenay Fjord (Quebec): a Holocene paleoseismicity record. *Quatern. Sci.*
865 *Rev.,* **23**, 283-294.

866 Steel, R.J. and Olsen, T. (2002) Clinoforms, clinoform trajectory and deepwater sands. In: Sequence
867 Stratigraphic Models for Exploration and Production: Evolving Methodology, Emerging Models and
868 Application Histories (Eds J.M. Armentrout, N.C., Rosen) GCS-SEPM Special Publication 22, 367-381.

869 Steel, R.J., Carvajal, C., Petter, A.L. and Uroza, C. (2008) Shelf and shelf-margin growth in scenarios of
870 rising and falling sea level. In: *Recent Advances in Models of Siliciclastic Shallow-Marine Stratigraphy* (Ed
871 G.J. Hampson) *SEPM Spec. Publ.,* 90, 47-71.

872 Steel, R., Mellere, D., Plink-Björklund, P., Crabaugh, J., Deibert, J., Loeseth, T. and Shellpeper, M. (2000)
873 Deltas v rivers on the shelf edge: their relative contributions to the growth of shelf-margins and basin-
874 floor fans (Barremian and Eocene, Spitsbergen). *GCSSEPM 20th Ann. Res. Conf. Spec. Publ.,* 981 – 1009.

875 Stevenson, C., Jackson C. A.-L., Hodgson, D.M., Hubbard, S.M. and Eggenhuisen, J.T. (2015) Deep-water
876 sediment bypass. *J. Sed. Res.,* **87**, 1058-1081.

877 Sumner, E.J., Talling, P.J., Amy, L.A., Wynn, R.B., Stevenson, C.J. and Frenz, M. (2012) Facies architecture
878 of individual basin-plain turbidites: Comparison with existing models and implications for flow
879 processes. *Sedimentology*, **59**, 1850-1887.

880 Sylvester, Z., Deptuck, M.E., Prather, B.E., Pirmez, C. and O'Byrne, C. (2012), Seismic stratigraphy of a
881 shelf-edge delta and linked submarine channels in the northeastern Gulf of Mexico. In: Application of
882 the Principles of Seismic Geomorphology to Continental-Slope and Base-of-Slope Systems: Case Studies
883 from Seafloor and Near-Seafloor Analogues (Eds B.E. Prather, M.E., Deptuck, D. Mohrig, B. Van Hoorn, B.
884 and R.B. Wynn, R.B.). *SEPM Spec. Publ.*, 99, 31–59.

885 Ta, T.K.O., Nguyen, V.L., Tateishi, M., Kobayashi, I., Saito,Y. and Nakamura, T. (2002) Sediment facies and
886 Late Holocene progradation of the Mekong River Delta in Bentre Province, southern Vietnam: an
887 example of evolution from a tide-dominated to a tide- and wave-dominated delta. *Sed. Geol.,* **152**, 313-
888 325.

889 Talling, P.J. (2014) On the triggers, resulting flow types and frequencies of subaqueous sediment density
890 flows in different settings. *Mar. Geol.,* **352**, 155-182.

891 Taylor, A.M. and Goldring, R. (1993) Description and analysis of bioturbation and ichnofabric. *J. Geol.*
892 *Soc.,* **150**, 141-148.

893 Tinterri, R. (2007) The Lower Eocene Roda Sandstone (South-Central Pyrenees): An example of a flood-
894 dominated river-delta system in a tectonically controlled basin. *Rivista Italiana di Paleontologia e*
895 *Stratigrafia*, **113**, 223-255. Vakarelov, B.K. and Ainsworth, R.B. (2013) A hierarchical approach to

architectural classification in marginal-marine systems: bridging the gap between sedimentology and sequence stratigraphy. *AAPG Bull.,* **97**, 1121-1161.

Van Lunsen, H. (1970) Geology of the Ara-Cinca region, Spanish Pyrenees, province of Huesca: Geologica Utraiectana, **16**, 1-119.

Van Wagoner, J.C., Mitchum, R.M. Jr., Campion, K.M. and Rahmanian, V.D. (1990) Siliciclastic sequence stratigraphy in well locations, cores and outcrops: concepts for high-resolution correlation of time and facies. *AAPG, Methods Explor.,* **7**, 55.

Vergés, J. and Muñoz, J.A. (1990) Thrust sequences in the southern Central Pyrenees: Bulletin de la Societe Geologique de France, **8**, 265-271.

Wadsworth, J.A. (1994) Sedimentology and Sequence Stratigraphy in an Oversteepened Ramp Setting: Sobrarbe Formation, Ainsa Basin, Spanish Pyrenees. Unpublished Ph.D. Thesis, University of Liverpool, p. 195.

Walker, R.G. (1967) Turbidite sedimentary structures and their relationship to proximal and distal depositional environments. *J. Sed. Petrol.*, **37**, 25-43.

Walker, R.G. and Plint, A.G. (1992) Wave- and storm-dominated shallow marine systems. In: *Facies Models: Response to Sea-level Change* (Eds R.G. Walker and N.P. James). *Geol. Assoc. Canada*, 219–238 pp.

Williams, P.F. and Rust, B.R. (1969) The sedimentology of a braided river. *J. Sed. Petrol.,* **39**, 649-679.

Wright, L.D., Yang, Z.-S., Bornhold, B.D., Keller, G.H., Prior, D.B. and Wiseman Jr., W.J. (1986) Hyperpycnal plumes and plume fronts over the Huanghe (Yellow River) delta front. *Geo-Mar. Letters*, **6**, 97-105.

Wright, L.D., Wiseman, W.J., Bornhold, B.D., Prior, D.B., Suhayda, J.N., Keller, G.H., Yang, L.S. and Fan, Y.B. (1988) Marine dispersal and deposition of Yellow River silts by gravity-driven underflows. *Nature* **332**, 629- 632.

Wright, L.D., Wiseman Jr., W.J., Yang, Z.S., Bornhold, B.D., Kneller, B.C., Prior, D.B. and Suhayda, J.N. (1990) Processes of marine dispersal and deposition of suspended silts off the modern mouth of the Huanghe (Yellow) River. *Cont. Shelf Res.,* **10**, 1-40.

Zavala, C., M., Arcuri, M. Di Meglio, H., Gamero, D. and Contreras, C. (2011) A genetic facies tract for the analysis of sustained hyperpycnal flow deposits. In: *Sediment transfer from shelf to deep water—Revisiting the delivery system* (Eds R.M. Slatt and C. Zavala) *AAPG Stud. Geol.,* **61**, 31–51.

Zavala, C., Arcuri, M. and Blanco Valiente, L. (2012) The importance of plant remains as diagnostic criteria for the recognition of ancient hyperpycnites. *Revue de Paléobiologie*, **11**, 457-469.

Zavala, C. and Arcuri, M. (2016) Intrabasinal and extrabasinal turbidites: origin and distinctive characteristics. *Sed. Geol.,* **337**, 36-54.

Zeng, J., Lowe, D.R., Prior, D.B., Wiseman Jr., W.J. and Bornhold, B.D. (1991) Flow properties of turbidity currents in Bute Inlet, British Columbia. *Sedimentology,* **38**, 975-996.

TABLE AND FIGURE CAPTIONS

Table Captions

Table 1: Descriptions and interpretations of shelf and slope facies associations (Facies Association A to Facies Association F).

Figure Captions

1. Map showing the location of the Ainsa Basin and the key neighbouring structural features, within the geological setting of the northern-Spanish South Pyrenean Foreland Basin. The dashed box shown in white, located in the Ainsa Basin, illustrates the area of study within the Sobrarbe Deltaic Complex. Line X–X^{I} indicates the location of the approximately dip-parallel outcrop transect sampled in this investigation. Adapted from Dreyer *et al.* (1999).

2. Simplified geological map of the study area. Line X–X^{I} shows the location of Las Gorgas Cycle 1 (Cycle LG-1), which is the dip-parallel outcrop transect sampled in this investigation. Line A–A^{I} shows a regional dip-parallel cross-section as shown in Fig. 3.

3. Regional cross-section showing the Sobrarbe Deltaic Complex stratigraphy (Line A–A^{I}; Fig. 2). The Sobrarbe Deltaic Complex is comprised of the uppermost part of the San Vicente Formation, the Sobrarbe Formation and up to the middle part of Mondot Member of the Escanilla Formation. The Sobrarbe Formation comprises several composite sequences: Comaron, Las Gorgas, Baranco el Solano and Buil. Highlighted in the burgundy box is line X–X^{I} (see Fig. 4), which is the study site of this investigation (Cycle LG-1). A simplified facies distribution is overlain. Adapted from Dreyer *et al.* (1999).

4. (A) Outcrop model constructed from unmanned aerial vehicle (UAV) photographs showing the study site (line X–X^{I} in Fig. 3); the upper and lower bounding surfaces of Cycle LG-1 are highlighted in yellow. The sedimentary log locations and sampling transects are highlighted in blue and are numbered. (B) Total log thickness at each logging and sampling location.

5. Pie charts illustrating differences in grain-size composition between Facies A to E. Sample numbers for each facies are shown in Fig. 6A. Facies A = fluvial channel-fill deposits; Facies B = delta top overbank deposits; Facies C = very fine-grained clean turbidites; Facies D = fine-grained micaceous turbidites; Facies E = medium-grained, deformed turbidites.

961 **6.** Grain size and sorting for Facies A to E. (A) Box and whisker plot illustrating differences in grain
962 size between Facies A to E. (B) Box and whisker plot illustrating differences in sorting between
963 Facies A to E. Sample numbers for each facies are shown are in shown in (A). Facies A = fluvial
964 channel-fill deposits; Facies B = delta top overbank deposits; Facies C = very fine-grained clean
965 turbidites; Facies D = fine-grained micaceous turbidites; Facies E = medium-grained, deformed
966 turbidites.

967 **7.** Sedimentary logs showing stratigraphic and dip-parallel facies distributions in Cycle LG-1. The
968 inset shows an enlarged grain-size scale: c = clay; s = silt; vf = very fine-grained sand; f = fine-
969 grained sand; m = medium-grained sand; c = coarse-grained sand; vc = very coarse-grained sand;
970 g = gravel; b = boulders.

971 **8.** Representative facies photographs. (A) Lenticular sand-body geometry (Facies Association A –
972 FA A). (B) Close-up of channel-fill within lenticular sand-body (FA A). (C) Trough cross-bedding
973 with uniformly dipping foresets (FA A); 0.32 m hammer for scale. (D) Sub-rounded granules and
974 pebbles of extraformational origin aligned parallel to stratification (FA A); marks on Jacob's Staff
975 denote 10 cm intervals. (E) Tabular sandstone beds, interbedded with structureless silt (Facies
976 Association B – FA B).

977 **9.** Representative facies photographs (Facies Association C – FA C). (A) Tabular beds of plane-
978 parallel laminated, very fine-grained, quartz-rich, clean sandstone. (B) Structureless
979 Foraminifera-dominated bioclastic sandstone (found in Location 2; see Figs 4 and 7); lens cap for
980 scale. (C) Normally graded Foraminifera-dominated bioclastic sandstone (found in Locations 3 to
981 6; see Figs 4 and 7); arrow indicates fining direction. (D) Foraminifera aligned parallel to
982 laminations (found in Locations 3 to 6; see Figs 4 and 7); 50 mm diameter lens cap for scale.

983 **10.** Basinward trends in grain size and sorting for Facies A to E of Cycle LG-1. Sampling locations are
984 illustrated in the numbered boxes. Sample numbers for each facies are shown in Fig. 6A.

985 **11.** Representative facies photographs (Facies Association D – FA D). (A) 0.75 to 1.5 m thick fine-
986 grained sandstone beds, note the micaceous appearance; hammer for scale. (B) 0.5 m thick beds
987 of Facies Association E – FA E, interbedded with 0.25 m thick siltstone beds. (C) Concave upward
988 bed-base with aligned mudstone rip-up clasts; lens cap for scale (50 mm diameter). D) Plane-
989 parallel laminated sandstone.

990 **12.** Representative facies photographs (Facies Association E – FA E). (A) 4 m thick medium-grained
991 sandstone bed, with erosive base cutting into underlying deposits; human for scale , *ca* 1.8 m
992 tall. (B) Contorted units; 1.5 m Jacob's Staff for scale. (C) Ball and pillow deformation structures;
993 marks on Jacob's Staff denote 10 cm intervals. (D) Trough cross-stratification; 0.2 m notebook
994 for scale.

995 **13.** Grain-size cumulative frequency plot showing basinward changes in grain size at each sampling
996 location.

997 **14.** Basinward trends in grain-size and sorting data. (A) Box and whisker plots showing basinward
998 changes in grain size at each sampling location. (B) Box and whisker plots showing basinward
999 changes in sorting at each sampling location.

1000 **15.** Clinothem model based on Cycle LG-1, including schematic grain-size logs; both grain size and
1001 the distribution of sand and mud vary downdip and through the stratigraphy at an intra-
1002 clinothem scale. Variability occurs according processes operating in the shelf, including the
1003 dominant process-regime in operation at the shelf-edge (interpreted to relate to autogenic river
1004 avulsion), and the flow style (i.e. sustained versus episodic hyperpycnal flows). Inferred bypass
1005 of the sustained hyperpycnal flows (Facies Association D – FA D) further downslope into the
1006 deep-water (basin-floor) environment is also illustrated.

1007

1008

1009

1010

1011

1012

1013

1014

Figure 1

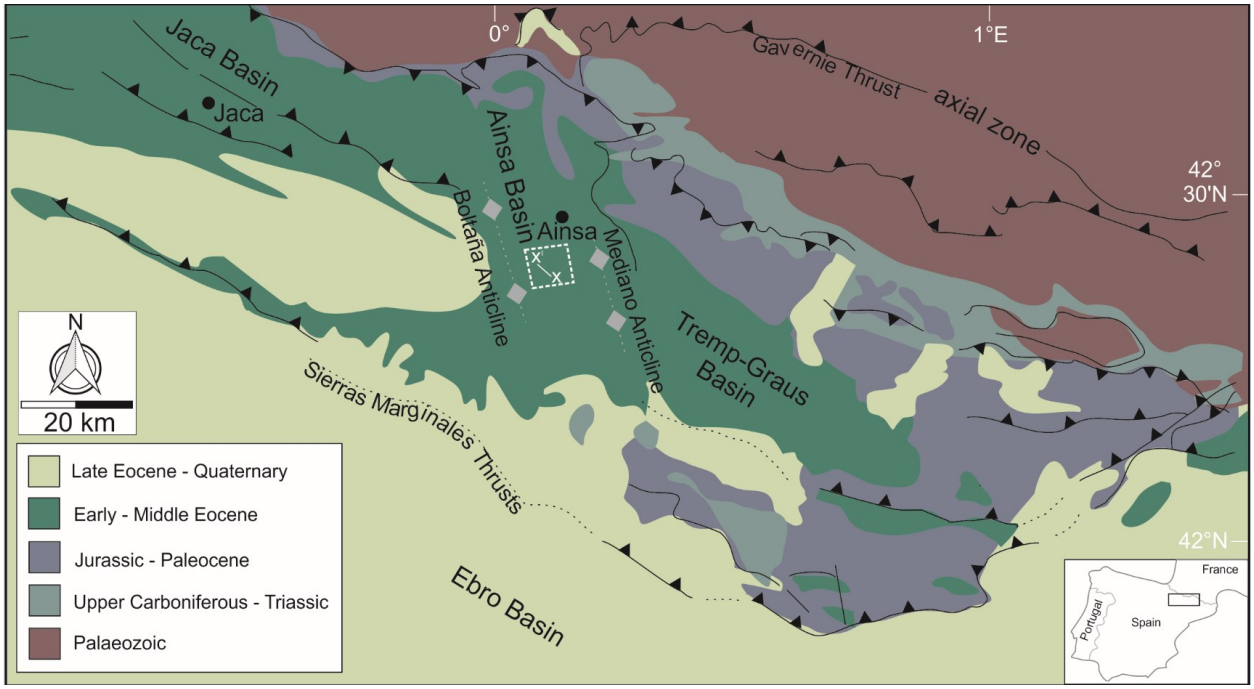
Jaca Basin
Jaca
0°
1°E
Gavernie Thrust
axial zone
42°
30'N
Ainsa Basin
Ainsa
Boltaña Anticline
Mediano Anticline
Tremp-Graus
Basin
Sierras Marginales Thrusts
Ebro Basin
42°N
N
20 km
Late Eocene - Quaternary
Early - Middle Eocene
Jurassic - Paleocene
Upper Carboniferous - Triassic
Palaeozoic
France
Spain
Portugal

Figure 2

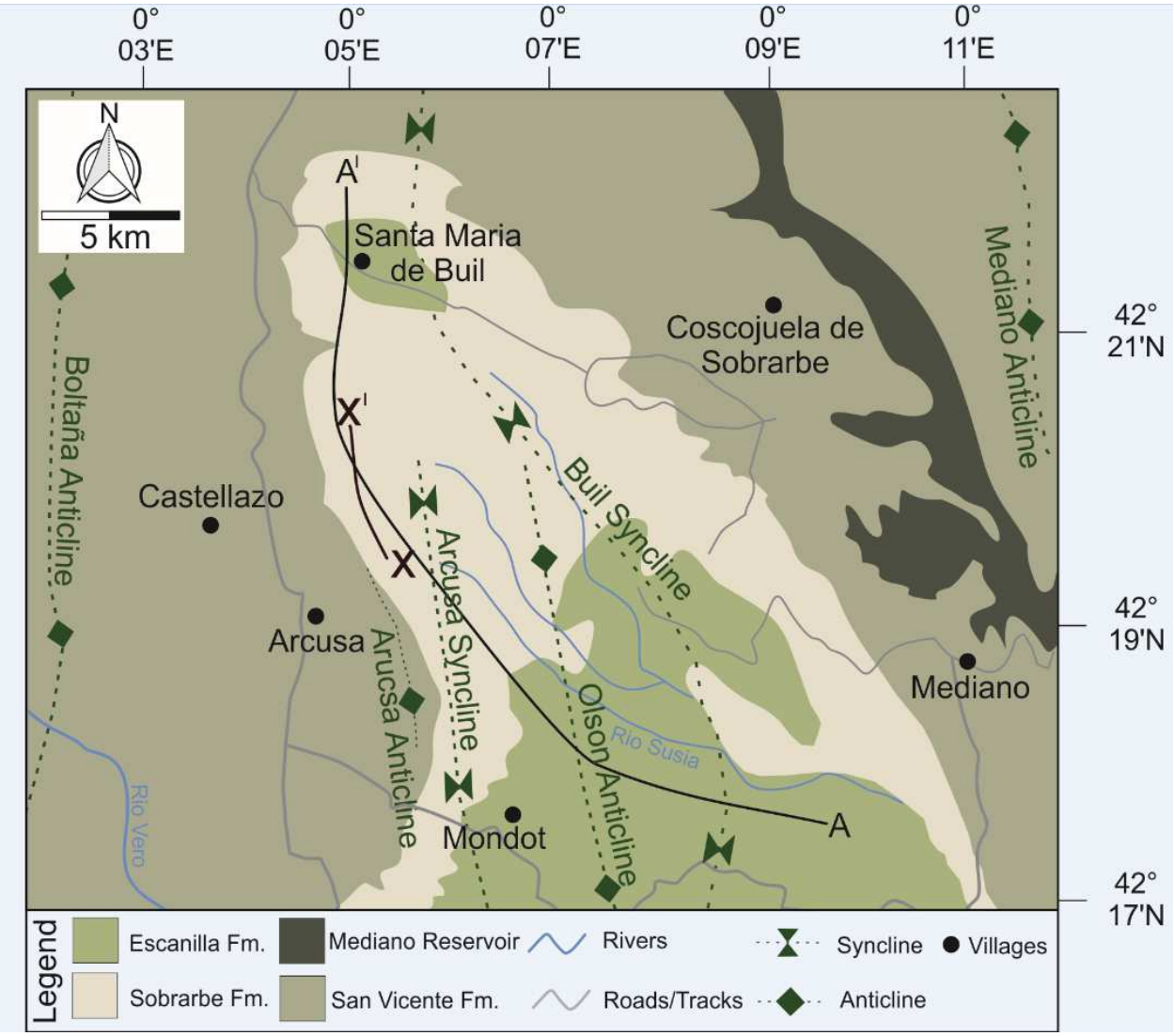
0° 03'E
0° 05'E
0° 07'E
0° 09'E
0° 11'E
N
5 km
A'
Santa Maria de Buil
Coscojuela de Sobrarbe
Mediano Anticline
42° 21'N
Boltaña Anticline
X'
Castellazo
Buil Syncline
Arcusa Syncline
X
Arcusa
Arucsa Anticline
Olson Anticline
Rio Susia
Mediano
42° 19'N
Rio Vero
Mondot
A
42° 17'N
Legend
Escanilla Fm.
Mediano Reservoir
Rivers
Syncline
Villages
Sobrarbe Fm.
San Vicente Fm.
Roads/Tracks
Anticline

Figure 3

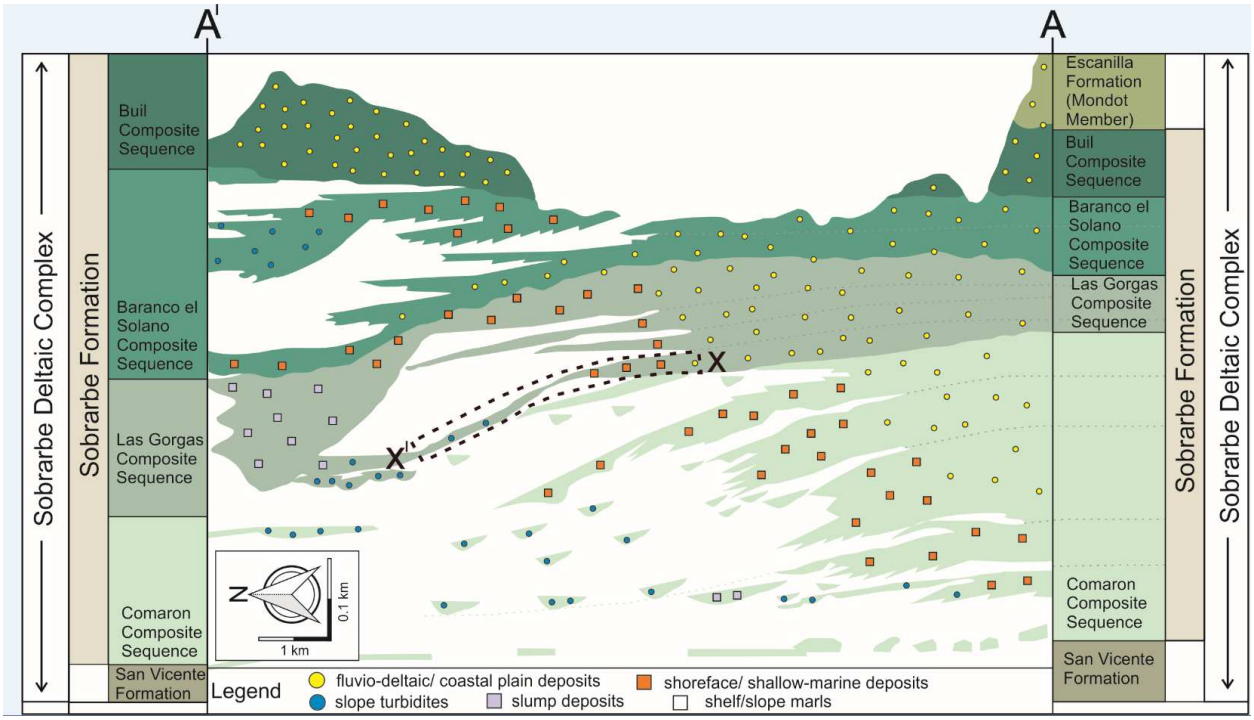
A'
A
Sobrarbe Deltaic Complex
Sobrarbe Formation
Buil Composite Sequence
Baranco el Solano Composite Sequence
Las Gorgas Composite Sequence
Comaron Composite Sequence
San Vicente Formation
Escanilla Formation (Mondot Member)
Buil Composite Sequence
Baranco el Solano Composite Sequence
Las Gorgas Composite Sequence
Comaron Composite Sequence
San Vicente Formation
Sobrarbe Formation
Sobrarbe Deltaic Complex
X
X'
N
0.1 km
1 km
Legend
fluvio-deltaic/ coastal plain deposits
shoreface/ shallow-marine deposits
slope turbidites
slump deposits
shelf/slope marls

Figure 4

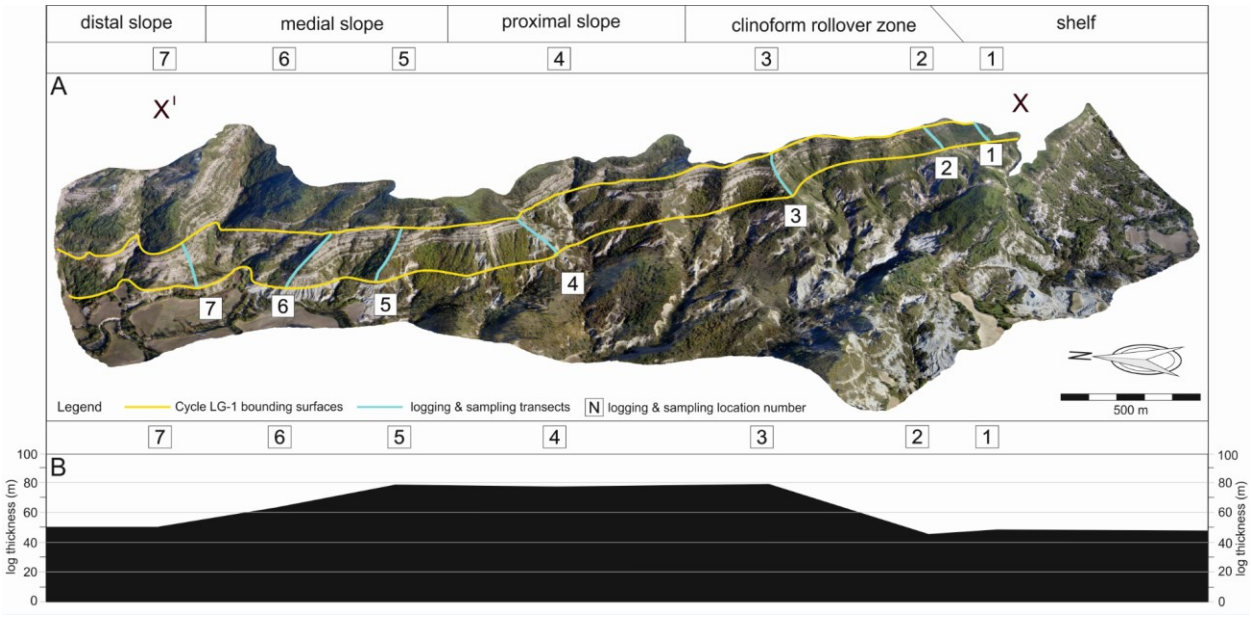
distal slope
medial slope
proximal slope
clinoform rollover zone
shelf
7
6
5
4
3
2
1
A
X'
X
Legend
Cycle LG-1 bounding surfaces
logging & sampling transects
N logging & sampling location number
500 m
B
log thickness (m)
100
80
60
40
20
0

Figure 5

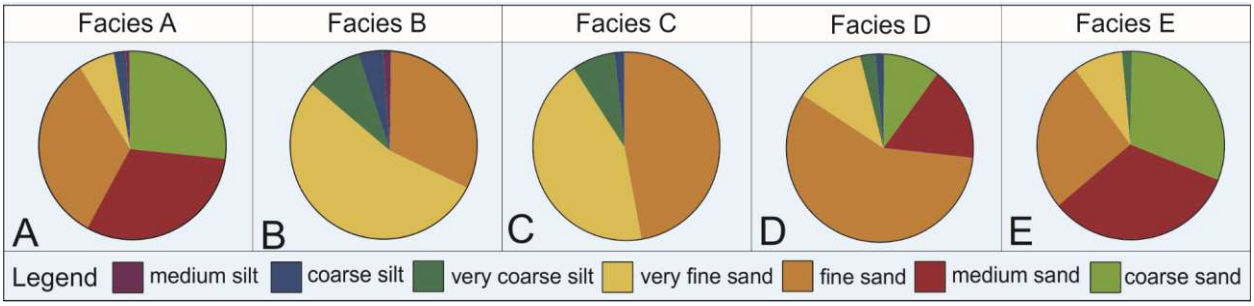
Facies A
Facies B
Facies C
Facies D
Facies E
A
B
C
D
E
Legend
medium silt
coarse silt
very coarse silt
very fine sand
fine sand
medium sand
coarse sand

1104 Figure 6

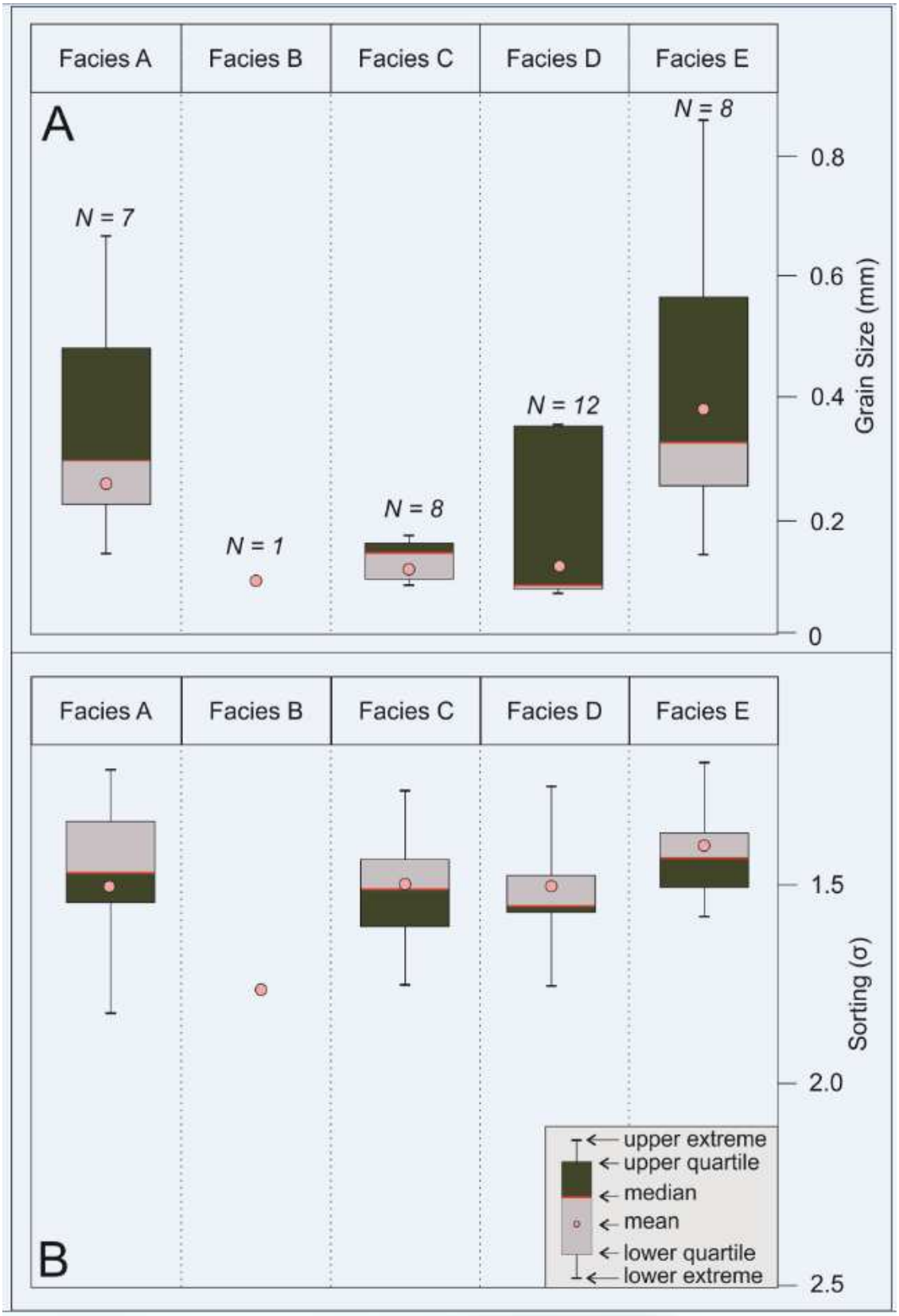

1105

Figure 7

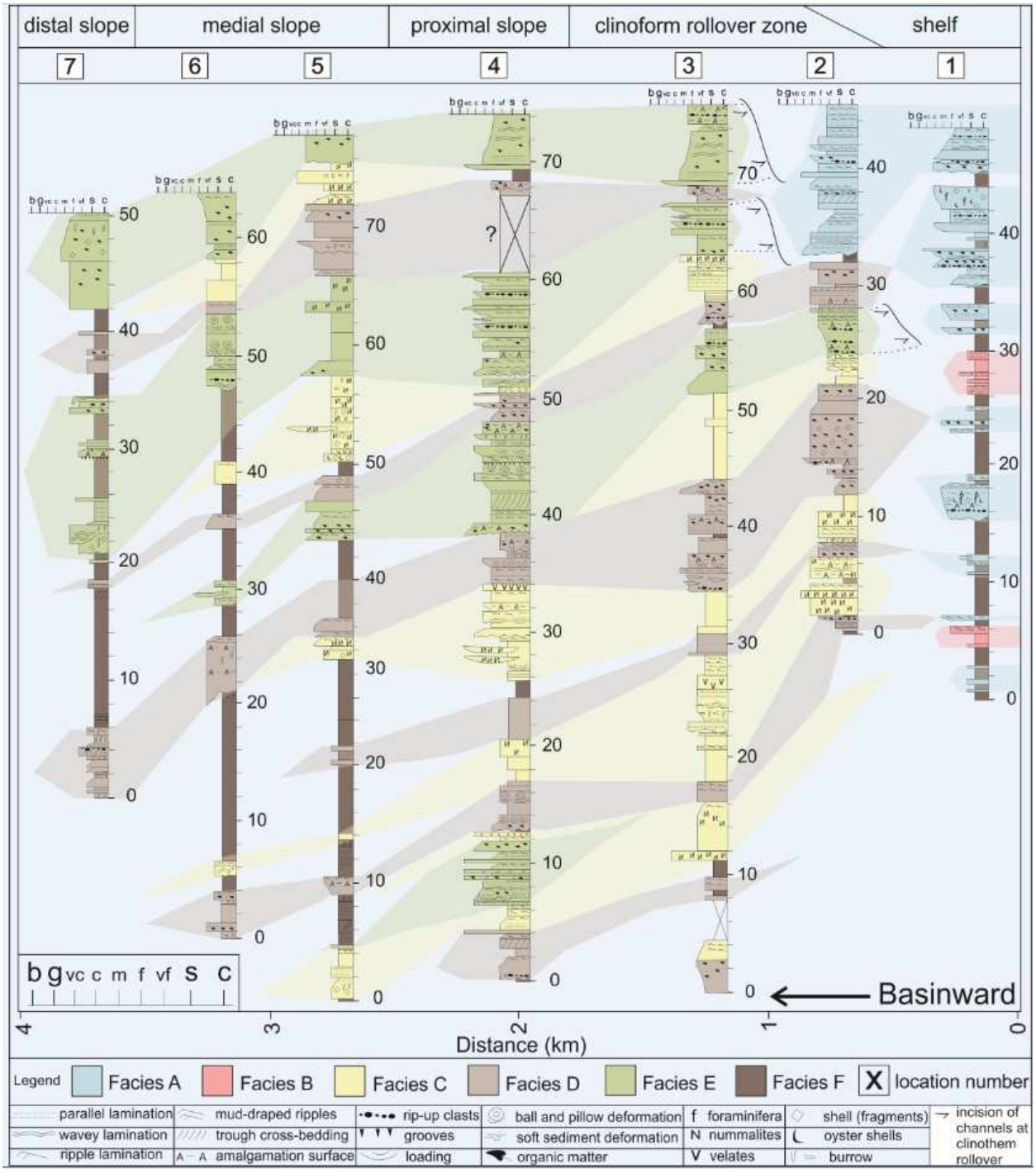
distal slope
medial slope
proximal slope
clinoform rollover zone
shelf
7
6
5
4
3
2
1
?
bg vc c m f vf s c
Basinward
Distance (km)
Legend
Facies A
Facies B
Facies C
Facies D
Facies E
Facies F
X location number
parallel lamination
wavey lamination
ripple lamination
mud-draped ripples
trough cross-bedding
A A amalgamation surface
rip-up clasts
grooves
loading
ball and pillow deformation
soft sediment deformation
organic matter
f foraminifera
N nummalites
V velates
shell (fragments)
oyster shells
burrow
incision of channels at clinothem rollover

Figure 8

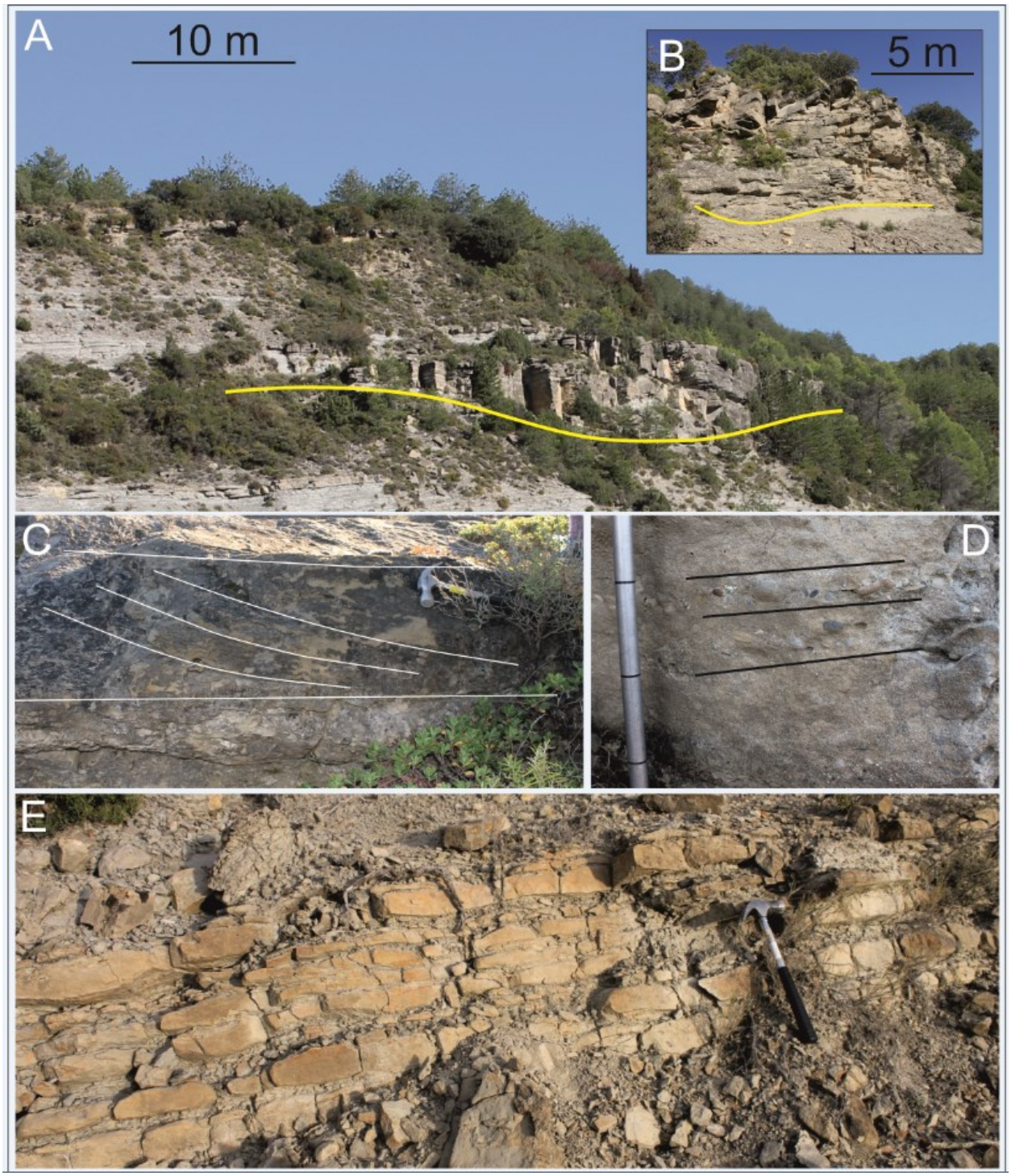

1117 Figure 9

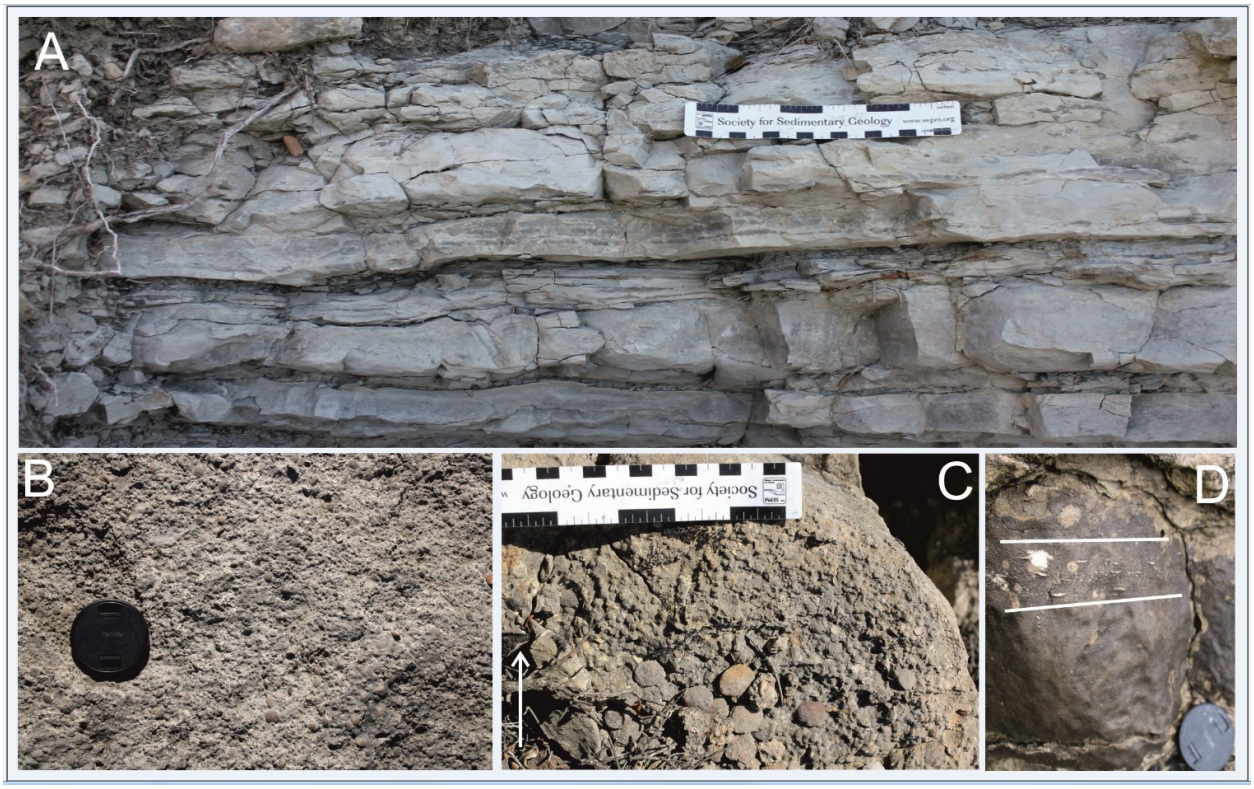

1118
1119
1120
1121
1122
1123
1124
1125
1126
1127
1128
1129
1130
1131
1132

Figure 10

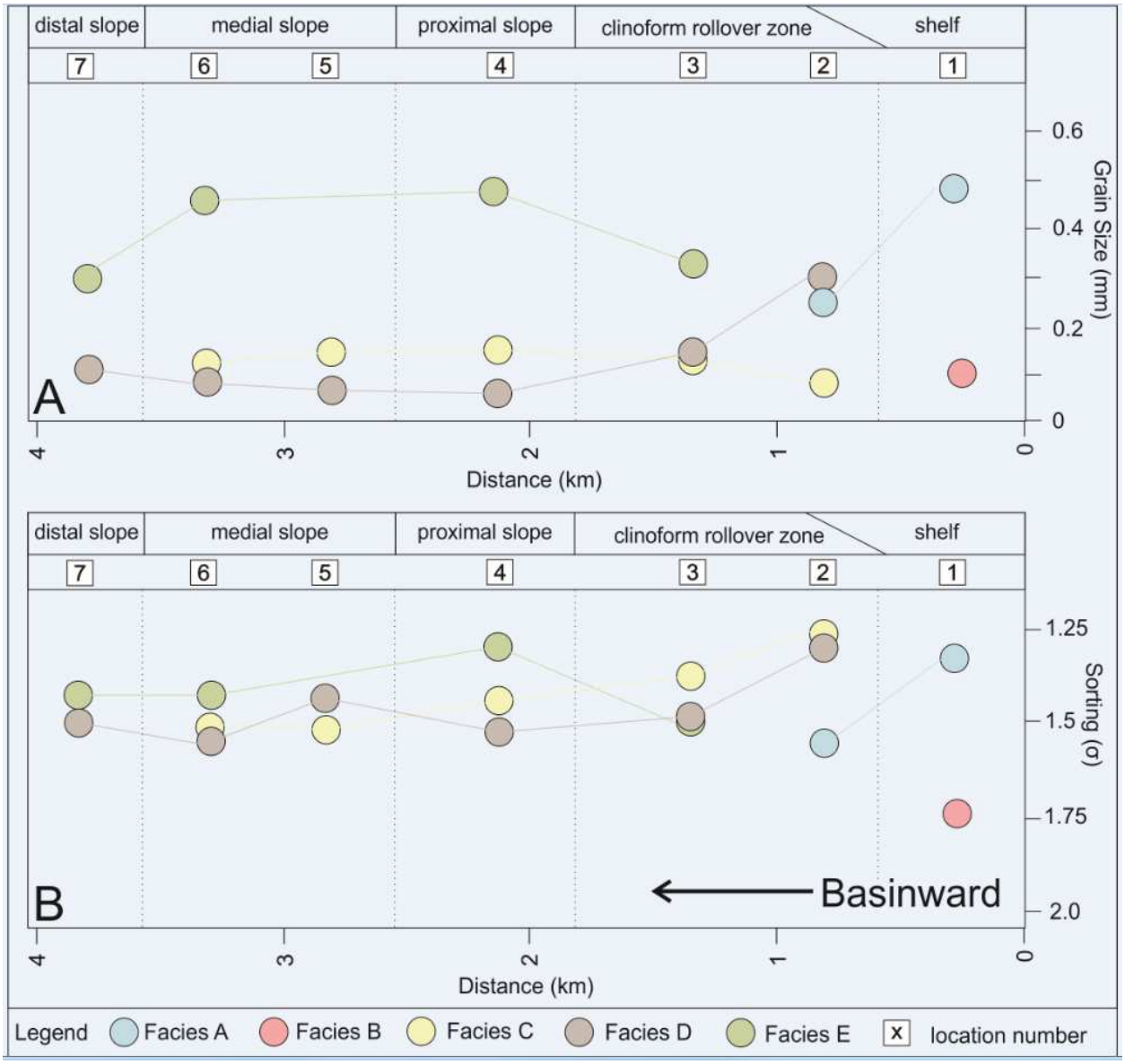
distal slope
medial slope
proximal slope
clinoform rollover zone
shelf
7
6
5
4
3
2
1
A
0.6
0.4
0.2
0
Grain Size (mm)
4
3
2
1
0
Distance (km)
B
1.25
1.5
1.75
2.0
Sorting (σ)
Basinward
Legend
Facies A
Facies B
Facies C
Facies D
Facies E
location number

Figure 11

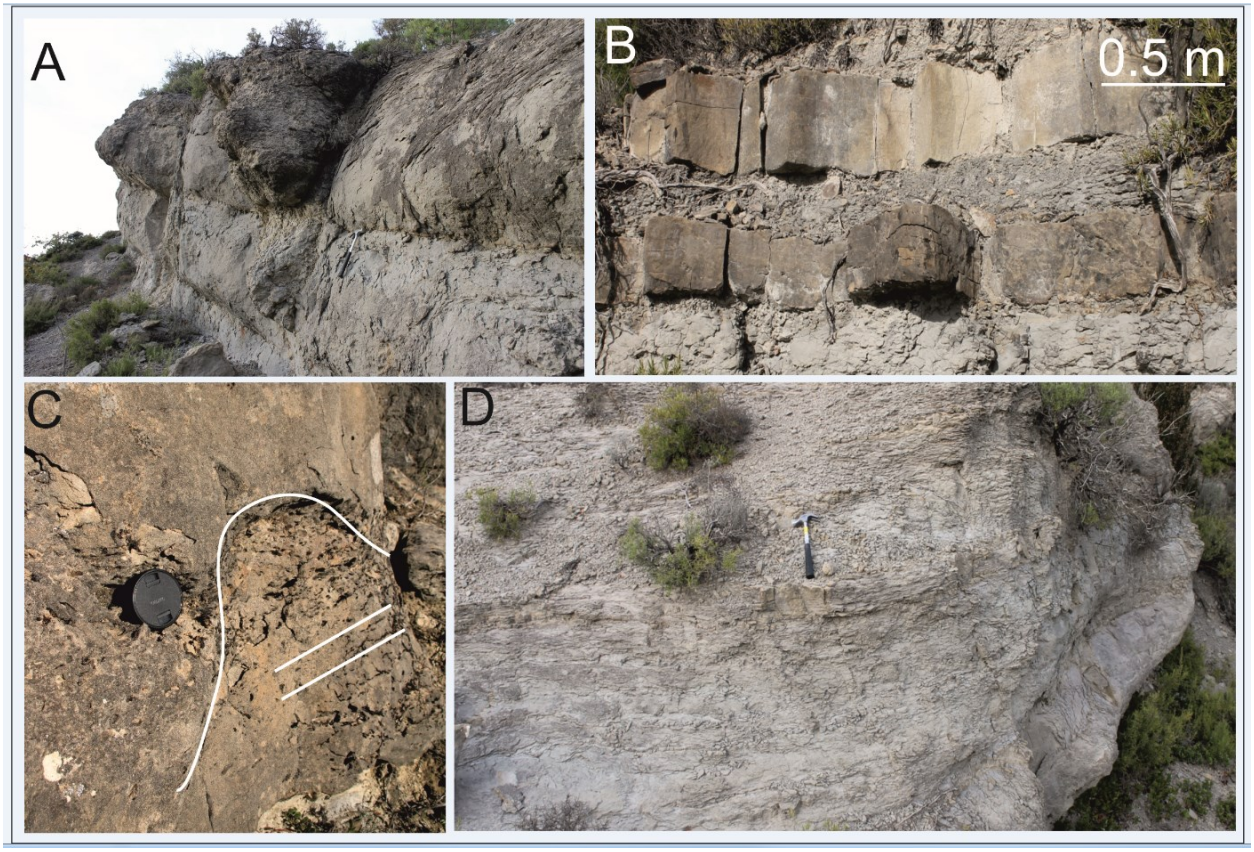

Figure 12

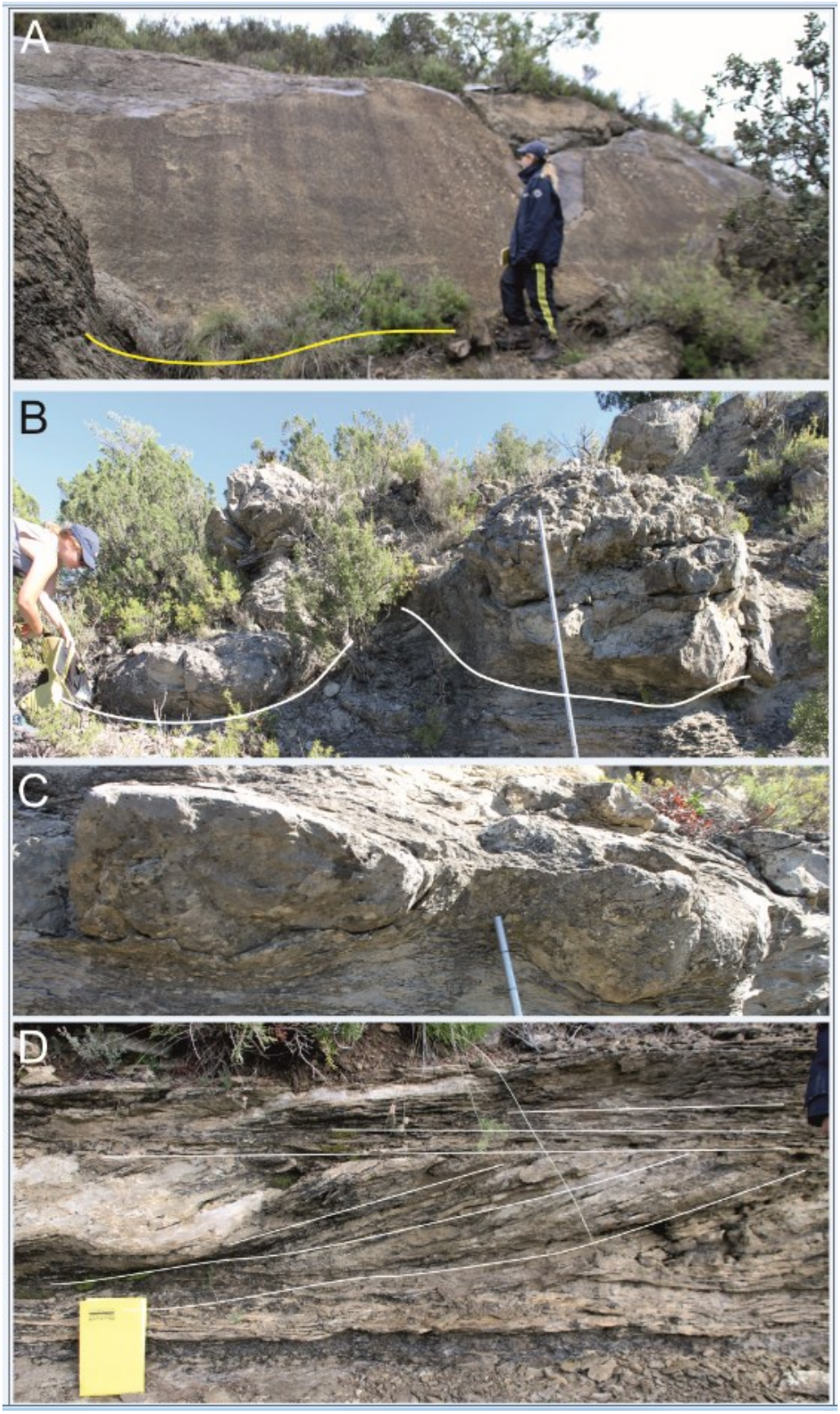
A
B
C
D

Figure 13

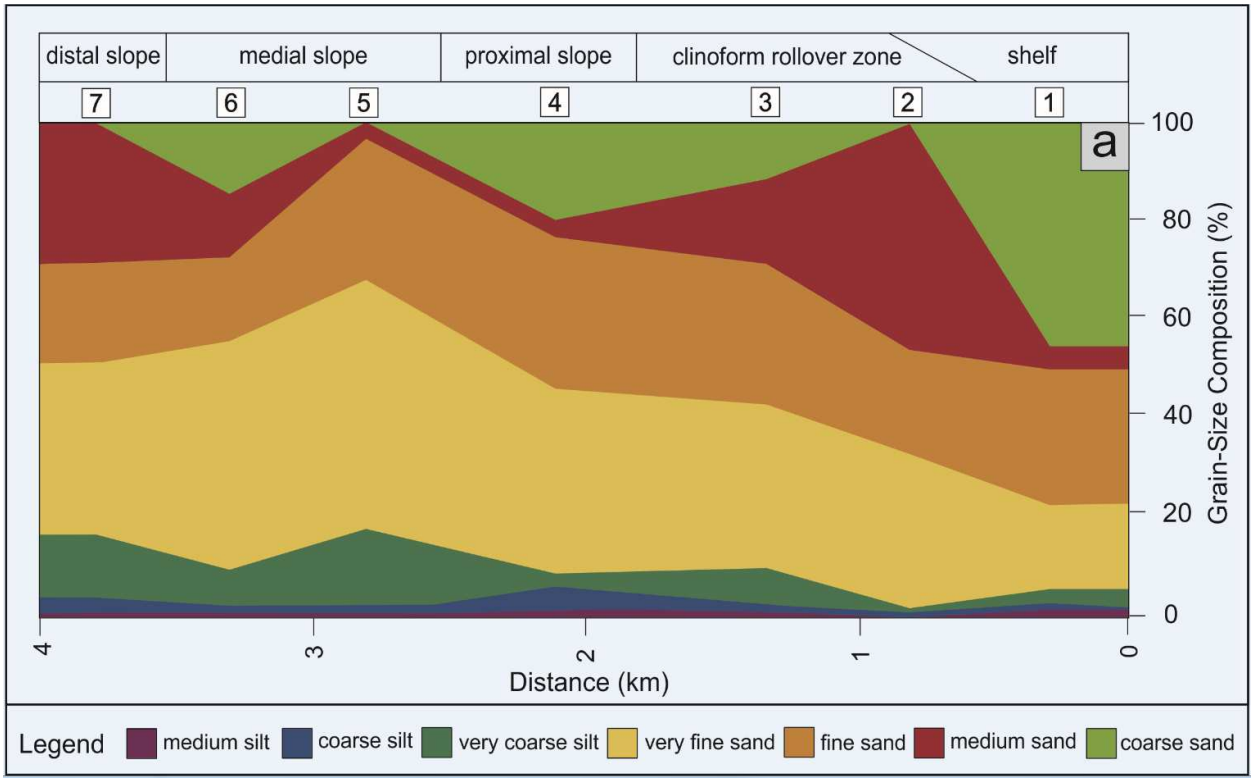
distal slope
medial slope
proximal slope
clinoform rollover zone
shelf
7
6
5
4
3
2
1
a
100
80
60
40
20
0
Grain-Size Composition (%)
4
3
2
1
0
Distance (km)
Legend
medium silt
coarse silt
very coarse silt
very fine sand
fine sand
medium sand
coarse sand

Figure 14

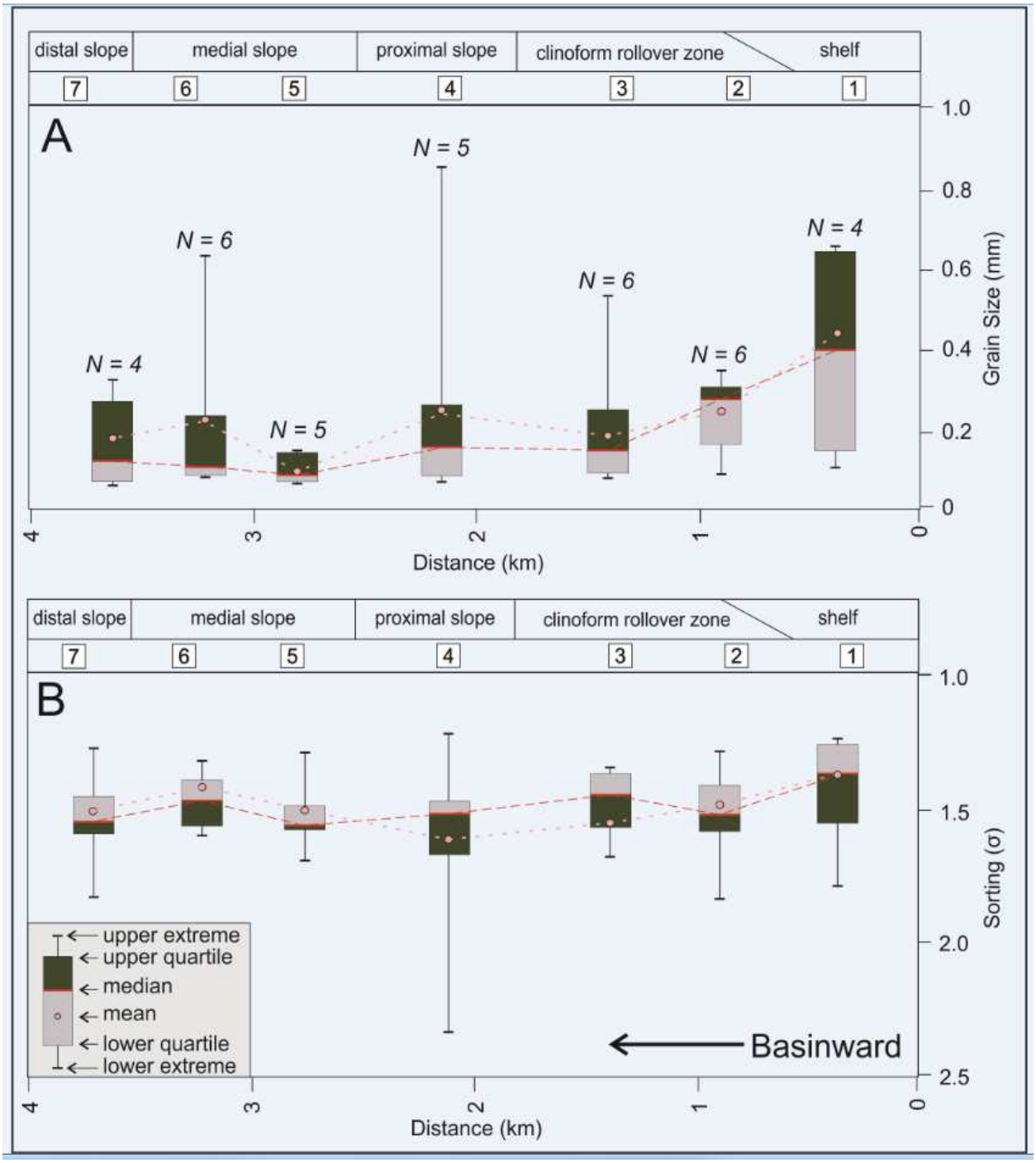
distal slope
medial slope
proximal slope
clinoform rollover zone
shelf
7
6
5
4
3
2
1
A
N = 4
N = 6
N = 5
N = 6
N = 6
N = 4
1.0
0.8
0.6
0.4
0.2
0
Grain Size (mm)
4
3
2
1
0
Distance (km)
B
1.0
1.5
2.0
2.5
Sorting (σ)
upper extreme
upper quartile
median
mean
lower quartile
lower extreme
Basinward
Distance (km)

1211 Figure 15

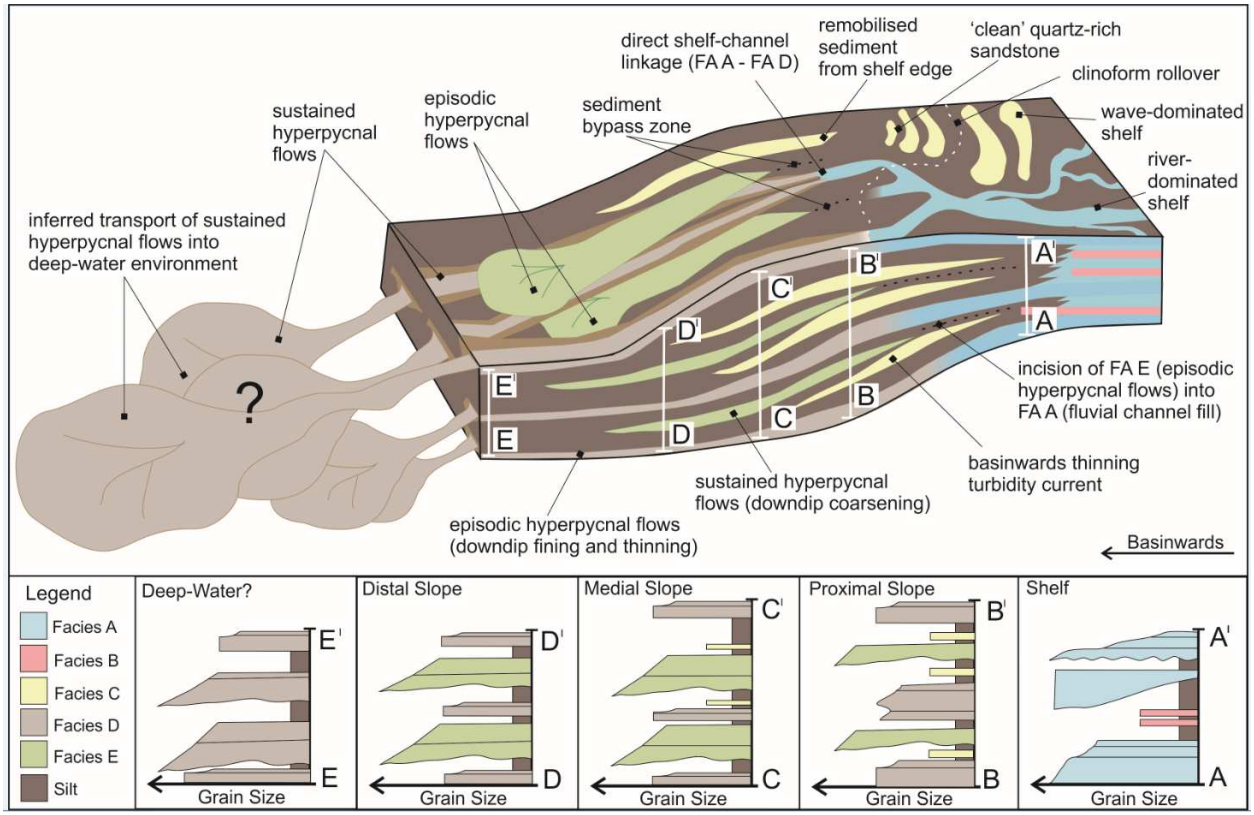

1212